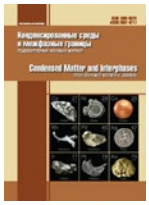

ISSN 1606-867X (Print)
ISSN 2687-0711 (Online)
Condensed Matter and Interphases
Kondensirovannye Sredy i Mezhfaznye Granitsy
https://journals.vsu.ru/kcmf/

Review

Review article
https://doi.org/10.17308/kcmf.2023.25/11256

Preparation, luminescence, and application of $LiMeBO_3$ borates, Me = Mg, Ca, Sr, Ba, Zn, Cd. Review

T. N. Khamaganova✉

Baikal Institute of Nature Management Siberian Branch of the Russian Academy of sciences
6 Sakhyanovoy st., Ulan-Ude, Buryatia, Russian Federation

Abstract

The review summarises and analyses data on the preparation, structure, and spectral-luminescent properties of $LiMeBO_3$-based borates, Me = bivalent metal.

These polycrystalline borates are prepared traditionally by solid-phase reactions and self-propagating high-temperature synthesis and its modifications based on a combustion reaction.

Frameworks of lithium borates with alkaline earth metals, zinc, and cadmium are formed from large metal polyhedra between which there are boron-oxygen triangles isolated from each other. Doping with rare-earth and heavy metal ions leads to the formation of solid solutions which normally have defective structures. Doped activator ions often become the main part of the luminescence centre in the phosphor. The luminescent properties of ions of rare-earth elements arise from the possibility of electronic transitions between states within the 4*f*-configuration. The paper discusses the most likely mechanisms of charge compensation during heterovalent substitution in $LiMeBO_3$ borates (co-doping and formation of cation vacancies). It is shown that charge compensation during the combined introduction of ions of REEs and alkali metals into the structure has a positive effect on the emission yield. The review considers the results of thermoluminescent, upconversion, and photoluminescent properties and processes and phenomena that cause them. It also explains the mechanism of resonance energy transfer from the sensitiser to the activator using the example of $Yb^{3+}\rightarrow Er^{3+}$.

It discusses the possibility of using the considered borates as phosphors that emit green, blue, and red light in white LEDs and as effective materials for personnel neutron dosimetry and the dosimetry of weak ionising radiation.

Keywords: Polycrystalline borates, Solid-phase synthesis, Combustion method, LEDs, Thermoluminescence, Green phosphor, Sensitisation

Funding: The study was supported by the Ministry of Science and Higher Education of the Russian Federation (the government order to the Baikal Institute of Nature Management, Siberian Branch of the Russian Academy of Sciences, project No. 0273–2021-0008).

For citation: Khamaganova T. N. Preparation, luminescence, and application of $LiMeBO_3$ borates, Me= Mg, Ca, Sr, Ba, Zn, Cd. Review. *Condensed Matter and Interphases.* 2023;25(3): 311–332. https://doi.org/10.17308/kcmf.2023.25/11256

Для цитирования: Хамаганова Т. Н. Получение, люминесценция и применение боратов $LiMeBO_3$, Me = Mg, Ca, Sr, Ba, Zn, Cd. Обзор. Конденсированные среды и межфазные границы. 2023;25(3): 311–332. https://doi.org/10.17308/kcmf.2023.25/11256

✉ Khamaganova T. N., e-mail: khama@binm.ru
© Khamaganova T. N., 2023

The content is available under Creative Commons Attribution 4.0 License.

1. Introduction

Lighting technology (residential and industrial, plasma and electroluminescent panels, mobile phones, displays, etc.) has been recently using white LEDs (w-LED) because of a number of advantages, i.e. reliability, high light efficiency, low energy consumption, environmental friendliness, and a long service life [1–3].

Developments in solid-state lighting have encouraged researchers to search for new efficient phosphors which can be used as sources of white light in LEDs. Ions of rare earth elements (REEs) and transition metals are used as activators in many inorganic phosphors (aluminates, vanadates, phosphates, etc.) due to the possibility to adjust their colour emission over a wide range of the visible spectrum [4-10].

Simple and complex borates are promising materials that meet the necessary requirements [3, 6, 8, 11–14]. Compounds of this class can be used as structural matrices of phosphors due to their high thermal and chemical stability, quantum efficiency, and crystallisation at relatively low temperatures [3, 6, 7]. They are characterised by high transparency in the visible region of the spectrum, a wide band gap, a high coefficient of thermal expansion, and strong absorption in the near ultraviolet region, which makes them excellent materials for optoelectronic devices, solid-state lighting, and data display devices [12–16].

In particular, due to ions of alkali and alkaline-earth metals, oxygen can be coordinated in borates in various ways, which results in various crystalline structures and allows finding new materials with excellent luminescent characteristics [3, 7, 12–20].

Recently, the problem of detecting and measuring radiation has become relevant. Methods based on the effects arising from the interaction of radiation with matter are used to record ionising radiation. Control of radiation doses is conducted with the help of sensors, whose action is based on the effect of thermally stimulated luminescence (TSL). TLD-600 (^{6}LiF:Mg,Ti) and TLD-700 (^{7}LiF:Mg,Ti) dosimeters have been successfully used for personnel neutron monitoring [21, 22]. However, they have many drawbacks, such as a complex structure of the glow curve, a complex annealing procedure, a loss of sensitivity when reused, and remaining residual signals [22, 23]. Therefore, it is necessary to search for and create new effective materials for these applications. Lithium borates are characterised by chemical resistance and stability, their synthesis is simple and relatively cheap and requires low temperatures [10, 13, 17]. These luminescent materials based on alkali and alkaline earth metal borates are promising for medical dosimetry due to the similarity of their effective atomic numbers to soft biological tissue (Z_{eff} = 7.4). Such materials are similar to it in terms of transmission and absorption of ionising radiation, which allows using them in individual, clinical, and radiobiological dosimetry of weak ionising radiation [24].

This paper systematises information on the synthesis, structures, and luminescent properties of lithium borates with bivalent metals of the following composition: $LiMeBO_3$, Me = Mg, Ca, Sr, Ba, Zn, Cd.

2. Methods for the preparation of LiMeBO3 lithium borates

Traditionally, the main method for the preparation of lithium borates of bivalent elements is solid-phase synthesis. It involves high-temperature sintering of lithium carbonate with metal carbonates (more rarely nitrates and fluorides) and boric acid [25–43]. $ZnLiBO_3$ borate is obtained by heating ZnO oxide with an excess of $LiBO_2$ at 800 ºC and extracting unreacted $LiBO_2$ in methanol [35].

Chang [44] prepared a single-phase polycrystalline sample of α-$LiZnBO_3$ by heating an equimolar mixture of $LiBO_2{\cdot}8H_2O$ and ZnO first at 620 ºC for 1 hour and then at 1,000 ºC for 12 hours. The authors [45] prepared α-$LiZnBO_3$ single-phase borate by annealing the same stoichiometric mixture of $LiBO_2{\cdot}8H_2O$ and ZnO at 600 °C for 1 month.

In [46], to prepare $LiZnBO_3$, a stoichiometric mixture of Li_2CO_3, ZnO, and H_3BO_3 was dissolved in diluted nitric acid. The solution was evaporated to remove water and nitric acid, heated at 600 °C and held for up to 3 weeks with intermediate homogenisation of the products. It was noted that the synthesised sample had a small amount of ZnO, which was associated with the volatilisation

of Li_2O during calcination. The authors of the work used a similar method to prepare $LiCdBO_3$ borate by keeping the mixture at 700 ºC, which was followed by quenching. In [47], $LiOH{\cdot}H_2O$ was used instead of Li_2CO_3 as the starting material and the heating temperature was 1,000 °C.

As a rule, solid-phase synthesis involves several stages and intermediate homogenisation of the products [48], for example, $LiMeBO_3$ (Me = Sr, Ba) was obtained by three-stage annealing [30]. The starting reagents for the $LiSrBO_3$ synthesis were Li_2CO_3, $SrCO_3$, and H_3BO_3, while $LiBaBO_3$ was synthesised from Li_2CO_3, BaF_2, and H_3BO_3. Annealing is sometimes conducted in a reducing atmosphere to prevent oxidation processes. For example, in [28], $LiSrBO_3$ phases: Eu^{3+}, Sm^{3+}, Tb^{3+}, and Dy^{3+} were prepared in air, while $LiSrBO_3$:Ce^{3+} was prepared in a reducing medium with a ratio of H_2:N_2 (5:95).

There is a growing number of publications dedicated to the synthesis of phosphors conducted by methods which result in the production of materials with nanoscale particles. For example, preparation of α-$LiZnBO_3$ by sol–gel technology [49]. It is known that this method is used to produce nanoscale particles and the process involves converting a liquid solution (hydrolysis and polycondensation) into a gel. The authors of the work dissolved the stoichiometric ratios of lithium nitrate, zinc (II) nitrate hexahydrate, and boric acid (1:1:1) in propionic acid. The resulting solution was stirred and heated at 100 °C to form a yellow gel. The gel was dried and the dried powder was heat treated at 700 ºC in an inert atmosphere. This resulted in the production of $LiZnBO_3$ borate particles of spherical shape.

In [50–56], the combustion method was proposed to be used to produce fine powders. In literature, depending on the reaction conditions this method is known as the method of self-propagating high-temperature synthesis (SHS) [54]. SHS is an autowave process that spontaneously propagates in a chemically active environment when the chemical reaction is localised in the combustion zone. It is used mainly for the production of inorganic materials: powders, pastes, ceramics, intermetallides, and refractory coatings. The SHS method differs from other methods involving high temperatures and short synthesis time since it allows controlling the process, has lower energy costs, and requires simple equipment [54, 55]. Among the varieties of self-propagating high-temperature synthesis are pyrohydrolytic synthesis, modified solid-phase diffusion method, and the Pechini process. These methods are universal and simple, the processes within them proceed quickly and allow obtaining various types of dispersed materials (including nanoscale) from simple binary compounds to complex doped phases. The process involves a self-sustaining reaction in a homogeneous solution of various oxidising agents (e.g., metal nitrates) and organic reducing agents (e.g., urea, glycine, hydrazine, citric acid, etc.). It is important that oxidation occurs in the absence of oxygen from the environment, but due to the fuel in the solution [56–58].

The Pechini process has been used to synthesise fine $LiMgBO_3$ powder [51]. For this, nitrate solutions of the corresponding metals and boric acid were separately prepared in deionised water. After they were mixed and sonicated, citric acid and ethylene glycol were slowly added to the resulting homogeneous solution at a molar ratio of 1:1 and 1:2, respectively. The solution was treated with nitric acid and evaporated to obtain a viscous yellow polymer resin. The resin was first dried at 200 °C and then annealed for 2–3 minutes at 550 °C. Remaining impurity traces were removed by sintering at 700 °C. Annealing of the resulting solid foamy black mass at 750 °C produced $LiMgBO_3$ nanoparticles. In this process, citric acid ($C_6H_8O_7$) and ethylene glycol (CH_2(OH) CH_2OH) were used as chelating and stabilising agents and fuels. The combustible agent and foaming agent was nitric acid (HNO_3). Similar conditions for the $LiMgBO_3$:Dy^{3+} synthesis were used in works [51, 52]. $CO(NH_2)_2$ urea can be used as a combustible material [59]. A study of the morphology of the surface of the $LiMgBO_3$:Dy^{3+} material synthesised by combustion showed that the shape of particles was irregular and their dimensions were within 5–10 μm [50]. The authors attributed a large number of cracks, voids, and pores on the surface to varying consumption of the mass during combustion.

A modified combustion method has also been used to obtain the considered borates [53, 58–65]. In [53], a simple and time-saving technology was used to produce $LiCaBO_3$:Tb^{3+}, which involved

preparing a mixture of lithium, calcium, and terbium nitrates and boric acid. Ammonium nitrate and urea were used as combustible materials. Fig. 1 presents a scanning electron microscope (SEM) image showing the morphology of the surface of the $LiCaBO_3:Tb^{3+}$ phosphor.

Due to the incongruent melting of $LiMeBO_3$ (Me = Zn, Cd), the solution-melt technology for growing crystals has become the most commonly used. Simple borates, such as $Li_2B_4O_7$, Bi_2O_3 bismuth oxide, and low-melting chlorides, for example, LiCl, BaF, were used as solvents.

The hydrothermal method allows obtaining $LiMeBO_3$ crystals, Me = Zn, Cd, at low temperatures from 250 to 450 °C [66-68].

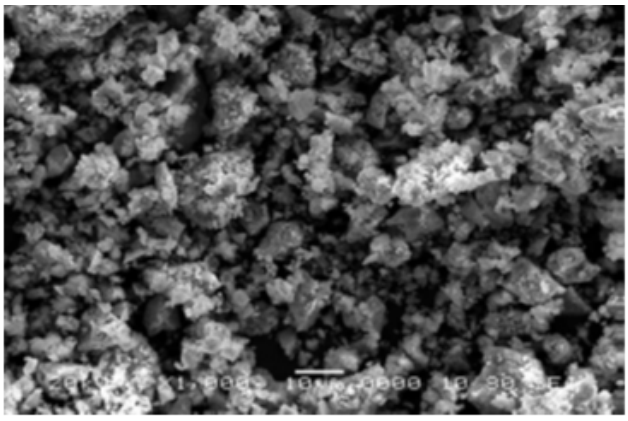

Fig. 1. SEM image of the $LiCaBO_3$:Tb3+ phosphor [53]

3. Crystalline structures of $LiMeBO_3$, Me = Mg, Ca, Sr, Ba, Zn, Cd

Crystallographic characteristics of $LiMBO_3$ obtained by X-ray diffraction analysis of single crystals are given in Table 1. It should be noted that this paper does not discuss in detail the structures of $LiMeBO_3$ with Zn, Cd since they will be considered in another article.

According to Norrestam, the structure of $LiMgBO_3$ determined by a single crystal is isotypical to the structure of monoclinic β-$LiZnBO_3$ [69]. The compound crystallises in the C2/c sp. gr. According to [69], Mg atoms are located in five-vertex polyhedra with Mg-O distances from 1.97 to 2.12 Å, and Li atoms are coordinated by four oxygen atoms with bond lengths from 1.88 to 2.33 Å and have trigonal-bipyramidal coordination. They are disordered and shifted from the central position by 0.3 Å above and below the trigonal plane.

Double borates $LiMBO_3$, M = Sr, Ba crystallise in the monoclinic crystal system and have one structural type [30]. In $LiSrBO_3$ and $LiBaBO_3$ structures, M atoms differ in their environment: CN(Sr) = 7 and CN(Ba) = 9. Li atoms are coordinated by five oxygen atoms and are inside distorted trigonal bipyramids. Boron atoms have

Table 1. Crystallographic characteristics of $LiMeBO_3$

M	Crystal system	Пр. гр	Lattice parameters, Å			α, β, γ, °	Z	Ref.
			a	b	s			
Mg	monocl.	C2/c	5.161(1)	8.880(2)	9.911(2)	β = 91.29(2)	8	[69]
Ca	rhomb.	Pbca	13.227(13)	6.167(16)	6.0620(6)		8	[31]
Sr	monocl.	$P2_1/n$	6.4800(13)	6.680(15)	6.8400(14)	β = 109.41(3)	4	[30]
Ba	monocl.	$P2_1/n$	6.372 (1)	7.022(3)	7.058 (1)	β = 113.89(1)	4	[30]
α-Zn	monocl.	C2/c	8.746(2)	5.091(1)	6.129(1)	β = 118.75(13)	4	[45]
α-Zn	tricl.	P-1	5.0915(9)	5.059(1)	6.156(1)	α = 65.81(1) β = 65.56(1) γ = 59.77(1)	8	[44]
β-Zn	monocl.	C2/c	5.094(1)	8.806(3)	10.374(4)	β = 91.09(3)	8	[68]
Zn	tricl.	P-1	5.0559(15)	6.097(2)	8.0359(18)	α = 75.75(2) β = 89.86(2) γ = 89.79(3)	4	[46]
I – Cd	hex.	P-6	6.324(2)		3.2638(7)		3	[66]
II – Cd	tricl.	P-1	6.118 (4)	8.486(3)	5.257(2)	α = 91.46(3) β = 89.64(4) γ = 104.85(4)	4	[67]
Cd	monocl.	$P\ 2_1/c$	10.4159 (14)	9.005(2)	10.756(2)	β = 92.521(13)	16	[46]

CN = 3 and an average distance B-O of 1.377 Å and O-B-O angles between 118.3(7) and 122.6(7) Å, which is typical for flat $(BO_3)^{3-}$ groups. The structures of the compounds are constructed from multiple [LiO]- and [MO]- layers isolated in the direction of [10-1], boron atoms are localised between the layers in the form of bridges. In [LiO]-layers, adjacent LiO_5 polyhedra form dimers connected by edges, wherein each dimer is linked with four adjacent dimers and forms two-dimensional sheets parallel to the diagonal *ac* plane.

The SrO_7 polyhedra in the $LiSrBO_3$ crystal were described as distorted single-capped trigonal prisms. In layers, SrO_7 polyhedra are linked by vertices and form chains that extend along the *b* axis. In turn, the adjacent chains are linked through oxygen atoms in the form of close-packed sheets parallel to the *ac* plane. Strontium-oxygen sheets, [LiO]-layers, are linked through oxygen atoms of BO_3 triangles along the [101] direction and form a three-dimensional framework. In the $LiBaBO_3$ double borate crystal, the BaO_9 polyhedra were described as distorted single-capped square antiprisms. In the [BaO] layers, the polyhedra form chains linked through common oxygen vertices. Similar to the $LiSrBO_3$ structure, the neighbouring chains of the Ba-polyhedra are linked through oxygen atoms and form close-packed sheets in the direction of the *b* axis. The sheets of Ba-polyhedra, [LiO]-layers, extend in the [10$\bar{1}$] direction and form a three-dimensional framework by means of bridging boron-oxygen atoms.

$LiCaBO_3$ borate crystallises in the orthorhombic crystal system (sp. gr. Pbca) [31]. Its crystalline structure consists of alternating [LiBO] and [CaO] layers elongated in the [100] direction. In the [LiBO]-layers, isolated $[BO_3]^{3-}$ groups are distributed along two directions: [011] and [01-1]. In the layers, the LiO_5 five-vertex polyhedra linked through common vertices are localised in the [011] and [0-11] directions and the BO_3 groups act as bridges. The projection of the $LiCaBO_3$ crystalline structure in the [001] and [100] directions is shown in Fig. 2. The average distances of 1.379 Å and the values of O–B–O angles between 119.19 (11) and 120.62 (8) are quite normal for flat BO_3 triangles. CaO_7 polyhedra form distorted single-capped trigonal prisms that are linked through edges and form layers parallel to the *bc* plane. Adjacent [CaO] layers are connected by flat boron-oxygen triangles. The crystalline structure of $LiCaBO_3$ differs from the structures of the other three compounds of alkaline earth metals $LiMBO_3$, M = Mg, Sr, Ba, which are monoclinic. In $LiMgBO_3$, flat BO_3 triangles are parallel to each other, while in structures with larger alkali metals they are neither parallel, nor perpendicular to each other [31]. The four studied structures have the same environment for the lithium atom, whose polyhedron was described as a distorted trigonal bipyramid.

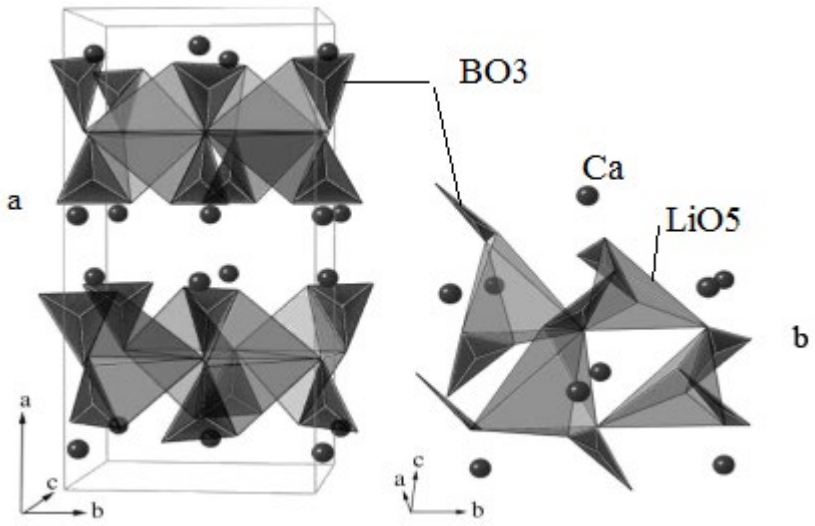

Fig. 2. $LiCaBO_3$ structure along [001] (a) and [100] (b) [31]

The structure of the monoclinic β-$LiZnBO_3$ crystal grown hydrothermally was established for the first time by Bondareva et al [68]. Chen et al. [45] named the structure of this modification as α-$LiZnBO_3$. It crystallises in the *C2/c* sp.gr., however, the parameters of its crystal lattice are different. The parameters of the unit cells of the $LiZnBO_3$ triclinic modification found in [44, 46] also differ. In the α-$LiZnBO_3$ structure, there are ZnO_4 tetrahedra, LiO_5 five-vertex polyhedra, and BO_3 triangles [45]. The two ZnO_4 tetrahedra connected by common edges form Zn_2O_6 dimers. Each Zn_2O_6 dimer connected by common O vertices with six other dimers forms a three-dimensional ZnO framework. The framework has hexagonal channels occupied by Li atoms and triangular voids occupied by boron atoms.

$LiMBO_3$ double borates, M = Cd, Zn, crystallise in 3 polymorphic modifications, their crystallographic characteristics are given in Table 1. The structural characteristics have been determined for two $LiCdBO_3$ modifications, low-temperature (triclinic, hexagonal [α-form]) and high-temperature (β-form). The $LiZnBO_3$ crystalline structures have been determined for triclinic and monoclinic modifications. Since the production of single crystals is challenging, the structure of the hexagonal low-temperature form has not been determined yet.

Therefore, crystals of isoformular $LiMBO_3$ lithium borates of alkaline earth metals belong to the lowest category and are characterised by triclinic, monoclinic, and rhombic crystal systems. Their framework structures include polyhedra of large metals and the available voids are occupied by boron-oxygen triangles isolated from each other.

3.1. Crystalline structures and luminescent properties of $LiMeBO_3$

Doping with metals

Mn^{2+} ions are important for creation of new luminescent materials since they are used to produce all known green phosphors [70]. Narrow-band red phosphors with an emission range of 620-650 nm for warm white LEDs are also being actively developed. Since the position of the lower excited state of Mn^{2+} strongly depends on the strength of the crystalline field, this will allow shifting the radiation of the Mn^{2+} substituted centres from green to red. A tetrahedral-coordinated Mn^{2+} ion with a weak crystalline field typically produces green radiation, while the octahedral coordinated Mn^{2+} (a strong crystalline field) produces orange-red radiation [70].

Inorganic materials doped with REE ions exhibit intense photoluminescence (PL) in the visible and infrared regions of the spectrum. Most lanthanide ions have luminescent properties, which is associated with the presence of *f–f* transitions [4–10, 62–63, 65, 71]. The intensity of PL lanthanide ions is determined by the efficiency of the occupation of excited states of Ln^{3+} and a decreasing probability of non-radiative processes. It depends significantly on a number of factors. For inorganic salts, the symmetry of the ions' environment and the absence of phonon quenching of photoluminescence are important factors for the intensity of PL. The peculiarities of the crystalline environment of the doped ion of REE affect the spectral-luminescent characteristics of the Ln^{3+} ion in the crystal (the position of its energy levels, the intensity of lines in the absorption and luminescence spectra) [9, 10, 20, 62, 70–76].

As the analysis of literature has shown, isovalent substitutions of cations of alkaline earth metals (Mg^{2+}, Ca^{2+}, Sr^{2+}, Ba^{2+}) for Mn^{2+}, Pb^{2+}, Eu^{2+} do not lead to fundamental changes in the structures of $LiMeBO_3$ borates. It is obvious that the introduction of a trivalent metal ion into the borate composition affects the valence balance. Ionic phases, which the considered borates can be attributed to, require the conditions of electroneutrality, i.e. the equality of the total positive and negative charges. There are various charge compensation mechanisms for crystalline phases with ionic bonds. Let us consider the most likely mechanisms of heterovalent substitutions applicable to $LiMeBO_3$ borates. In the case when the activator is a trivalent ion of REE, it is possible to substitute two identical atoms at equivalent positions with two different atoms of the same total valence. For example, codoping with a monovalent cation according to the scheme: $2Me^{2+} = R^{3+} + M^{+}$.

For instance, ions of alkali metals (Li^+, Na^+, K^+) have been used as charge compensators of lanthanide ions in a number of works [13, 14, 28, 32]. In all cases, the authors succeeded in

achieving electroneutrality and maintaining the crystalline structure. In the absence of charge compensators in the structure of the ionic crystal, vacancies in the cationic sublattice were formed. Many authors mention functional properties that are sensitive to the slightest changes in structure. However, this issue is hardly ever discussed and a detailed interpretation of the structure is hardly ever given. Very few works used the Rietveld method to determine the structure and occupied metal positions and to find correlations between the structure and photoluminescence [32, 74]. The results of interpretation of the $LiMgBO_3$:$x$$Tb^{3+}$ structure [74] in accordance with the data [69] showed the presence of two independent Li positions occupied by ~ 50% and one Mg position. In this structure, heavy metal atoms had CN=5 and were described as trigonal bipyramids (Fig. 3). Coordination of Li, B, and Mg atoms was confirmed by the IR spectra of the phases. The Li^+, Mg^{2+}, and Tb^{3+} ionic radii for CN = 6 were 0.76, 0.72, and 0.92 Å, respectively. The ionic radii and the charge difference between the dopant and the metal ions allowed assuming that Tb^{3+} could occupy both Mg^{2+} and Li^+ positions in the structure. However, clarification of the occupied positions indicated mixing of cations and a preference of Mg^{2+} positions over Li^+ positions in the $LiMgBO_3$ lattice. Since the difference in the Mg^{2+} and Tb^{3+} radii exceeded the difference in the Tb^{3+} and Li^+ radii, there was a high probability of a transition of Tb^{3+} at the Li^+ position. Then, the difference in their charges was +2 and new cationic vacancies of negative charge necessary for the balance of charges appeared. To study the local environment of $Tb3^+$, the photoluminescence lifetime was measured. The authors obtained two different lifetime values indicating two local environments of $Tb3^+$. It was assumed that $Tb3^+$ could be present in the lattice in two possible ways: either in two different points or in the same point, but with different surroundings defects. Since *f–f* transitions of Tb^{3+} are spin and parity forbidden, they can become permitted in an asymmetric position, i.e. a short lifetime may be due to the fact that Tb^{3+} occupies distorted positions of Li^+. The percentage of the short-lived component is only 8%, which indicates a low probability of this option. In contrast, the long-lived component, which is 92%, should be due to the high Tb^{3+}

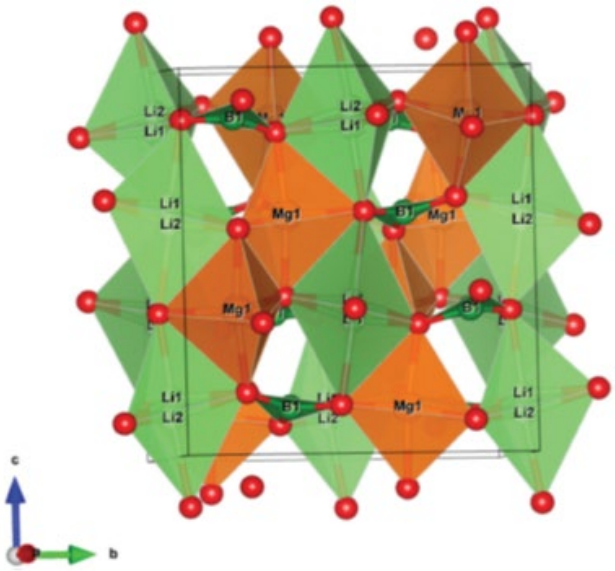

Fig. 3. $LiMgBO_3$ structure [74]

content in the symmetrical position of Mg^{2+}. The maximum peak intensity of the magnetic dipole transition at 545 nm in the emission spectra of all $LiMgBO_3$:$x$$Tb^{3+}$ phases confirms the fact that Tb^{3+} occupies the symmetric position of Mg^{2+} since the electric dipole transition line is permitted only in the case of its asymmetric position. Therefore, two different PL lifetime values may be due to two Tb^{3+} ions located at crystallographically identical positions of Mg^{2+} but with different surrounding defective centres. According to [75], some defective centres can act as electron-trapping centres and increase the lifetime, while others can provide non-radiative pathways to an excited state and reduce the lifetime value. The distances between such defective centres and lattice points affect the excited states [76]. For example, the short-lived component of PL can be located near defective centres, while the long-lived component can be far from them. The authors [74] noted that the values of short-lived and long-lived components of photoluminescence depend on the concentration of dopant, which determines the amount of charge imbalance in the initial matrix.

The formation of cationic vacancies for charge compensation was reported in [32] during the study of the luminescence of solid solutions of $LiSrBO_3$:Dy^{3+}, Tm^{3+}, Eu^{3+}. The authors emphasised that their work was focused on the behaviour of phases during energy transfer and colour adjustment, but it ignored the effect of the dopant concentration on LSBO. However, they identified

4 structures of $LiSrBO_3$ powders doped with each of these REE cations and with all three at the same time, they provided the coordinates of the atoms and their isotropic thermal parameters. It is interesting that the crystalline structures were specified in the $P2_1/c$ sp. gr. [32] and have acceptable divergence factors. However, according to the structural interpretation of the single crystal of a pure undoped compound, $LiSrBO_3$ borate crystallises in the $P2_1/n$ sp.gr. [30]. The authors referred to this work, but did not discuss this issue in any way. It was indicated that dopant cations occupied the positions of Sr^{2+}. Obviously, doping with REE ions leads to a noticeable distortion of the structure of the initial matrix and its reconstruction caused by the compensation of charges that occurs during the formation of new phases. The reconstruction of the structure is expressed in the changing symmetry of the crystals, which leads to the $P2_1/n \rightarrow P2_1/c$ sp.gr. transition. Emission spectra of the phases indirectly confirm the results of the determination of the structure. For example, in the radiation spectrum excited at 350 nm, there were bands at 490 nm (corresponding to the $^4F_{9/2} \rightarrow {}^6H_{15/2}$ transition of Dy^{3+}ions) and the most intense one at 576 nm (the $^4F_{9/2} \rightarrow {}^6H_{13/2}$ electric dipole transition permitted when Dy^{3+} is in a local position outside the inversion centre). This indicated that $Dy3^+$ ions occupied positions distant from the inversion centre in the $P2_1/c$ sp.gr. The same results were obtained for other REE ions.

The data [32, 74] further confirm that luminescence is a structurally sensitive method that is effective for characterising the features of the crystalline structure of the studied phases.

It is known that Eu^{3+} or Eu^{2+} ions when introduced into the lattices of various matrices emit perfectly fine in the blue and red regions of visible light and are actively used to develop various light-emitting devices [8, 63, 70]. Photoluminescence spectra of $LiMgBO_3:Eu^{3+}$ was investigated by Liang et al. [25]. When excited by near ultraviolet (UV) (395 nm) and visible light (466 nm), the studied sample exhibited intense red glow with λ = 615 nm, which corresponds to the $^5D_0 \rightarrow {}^7F_2$ forced electric-dipole transition of Eu^{3+} ions. When the $LiMgBO_3:Eu^{3+}$ sample was doped together with a sensitiser (Bi^{3+} ions), the absorbance of the $^7F_0 \rightarrow L_6$ and $^7F_0 \rightarrow {}^5D_2$ transitions increased. The authors attributed the increase in the luminescence intensity of the $LiMg_{0.75-y}BO_3:Eu_{0.25}{}^{3+}, Bi_y{}^{3+}$ sample to the $Bi^{3+} \rightarrow Eu^{3+}$ energy transfer. They believed that main energy transfer mechanism in the sample was the quadrupole-quadrupole interaction. The authors considered both new phosphors as pumping materials in the near UV range of the spectrum.

Dy^{3+} ions provided emission bands in the blue (480 nm) and yellow (570 nm) regions of the spectrum corresponding to the transitions: $^4F_{9/2} \rightarrow {}^6H_{15/2}$ magnetic dipole and $^4F_{9//2} \rightarrow {}^6H_{13/2}$ hypersensitive electric dipole transitions. Moreover, the intensity of the yellow glow was strongly influenced by the oxygen environment of the ion, which created a crystalline field of the host lattice and a radial integral of 4*f*- and 5*d*-electrons [60].

White light can be obtained by changing the intensity ratio of yellow and blue (Y/B) glow [1–5,70]. When excited in the near UV range, the phosphor emitted intense blue and yellow glow and a weak red band at 484, 573, and 669 nm, respectively, attributed to the $^4F_{9/2} \rightarrow {}^6H_{15/2}$, $^6H_{13/2}$, $^6H_{11/2}$ transitions of Dy^{3+} ions. The band gap width and average size of the material crystals were approximately 5.4 eV and 35 nm, respectively. The CIE chromaticity coordinates for $LiMgBO_3:0.02Dy^{3+}$ phosphor were in the white region, although they were far from the ideal values of the white light (0.333, 0.333) (see Table 2).

3.2. Thermoluminescence

All phosphors show a different thermoluminescent (TL) response to different types of exposure (X-, gamma-, ultraviolet rays, heavy ions) due to the unequal distribution of doses at different exposures [77]. The efficiency of luminescence and afterglow also depends on the method of material preparation, the chemical composition, and the particle size [71, 77, 78].

Work [79] describes dosimetric studies of $LiMgBO_3:Dy^{3+}$ exposed to X-rays [50], gamma rays, and C^{+5} heavy carbon ions [52], gamma radiation, and Ag^{9+} heavy silver ions with an energy of 120 MeV.

Work [50] studied the relationship between the TL response and the amount of absorbed

Table 2. Chromaticity coordinates and excitation wavelength in $LiMeBO_3$ borates

Material	Chromaticity coordinates (*x*, *y*)	λ_{ex} (nm)	Colour	Reference
$LiMgBO_3$:0.02Er^{3+},0.08Yb^{3+}	(0.6080, 0.3914)	980	orange	[65]
$LiMgBO_3$: 0.02Dy^{3+}	(0.45, 0.46)	348	white	[60]
$LiMgBO_3$: 0.01Tb^{3+} $LiMgBO_3$: 0.04Tb^3 $LiMgBO_3$: 0.06Tb^3	(0.32, 0.50) (0.29, 0.53) (0.39, 0.52)	235	green	[74]
$LiCaBO_3$: 0.02Dy^{3+} $LiCaBO_3$: 0.03Dy^{3+}	(0.35, 0.39) (0.35, 0.39)	351 351	white	[98]
$LiCaBO_3$: 0.005Tb^{3+}	(0.28, 0.71)	240	green	[53]
$LiSr_{0.995}BO_3$:0.005Ce^{3+} $LiSr_{0.955}BO_3$:0.005Ce^{3+},0.04 Tb^{3+} $LiSr_{0.915}BO_3$:0.005Ce^{3+},0.08 Tb^{3+} $LiSr_{0.875}BO_3$:0.005Ce^{3+},0.12 Tb^{3+}	(0.196, 0.242) (0.217, 0.282) (0.301, 0.412) (0.326, 0.423)	337	blue yellowish-green	[95]
$LiBaBO_3$:0.05 Ce^{3+}/0.02Mn^{2+}	(0.358, 0.251)	345	white	[34]
$LiBaBO_3$:0,02Er^{3+}, 0,08Yb^{3+}	(0.6060, 0.3914)	980	orange	[92]
$LiBa_{0.98}$ BO_3: 0.02Eu^{3+} $LiBa_{0.975}$ BO_3: 0.025Eu^{3+}	(0.368, 0.378) (0.376, 0.366)	354	white	[7]

dose for several samples. The authors compared thermoluminescence curves for $LiMgBO_3$:Dy^{3+} and commercial TLD–100 irradiated with 5 Gy. It was established that the glow curve of the material had a simple symmetrical shape of ~ 154 °C and, according to the peak shape method [80, 81], it obeyed first-order kinetics. The glow intensity was approximately half of the TL of the commercial TLD-100. The obtained linear dependence in a wide range of doses of 0.5–25 Gy indicated the good quality of the thermoluminescent material. Its disadvantage is a decrease in the luminescence intensity over time.

Fig. 4 shows thermoluminescence curves for different concentrations of Dy^{3+} in the $LiMgBO_3$:Dy^{3+} phosphor [52]. Kinetic parameters are given in Table 3. The samples' fading was studied by appropriate irradiation and exposure in the dark for 27 days (Fig. 5). After the samples were exposed to γ-rays and carbon rays, the fading

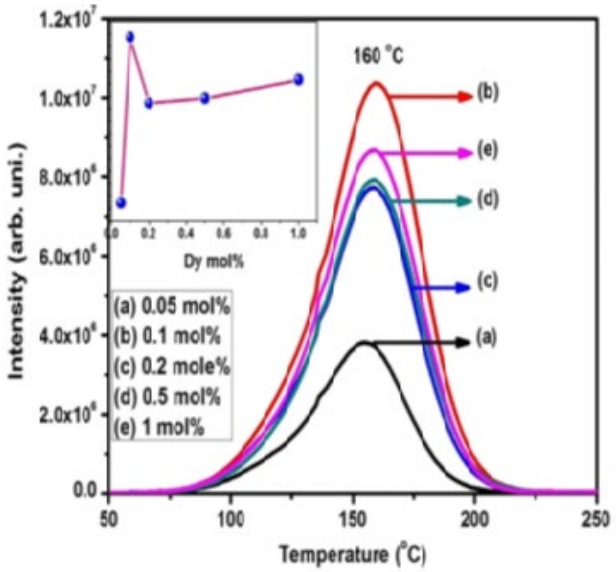

Fig. 4. Thermoluminescence curves for different concentrations of Dy^{3+} in the $LiMgBO_3$:Dy^{3+} phosphor according to [52]

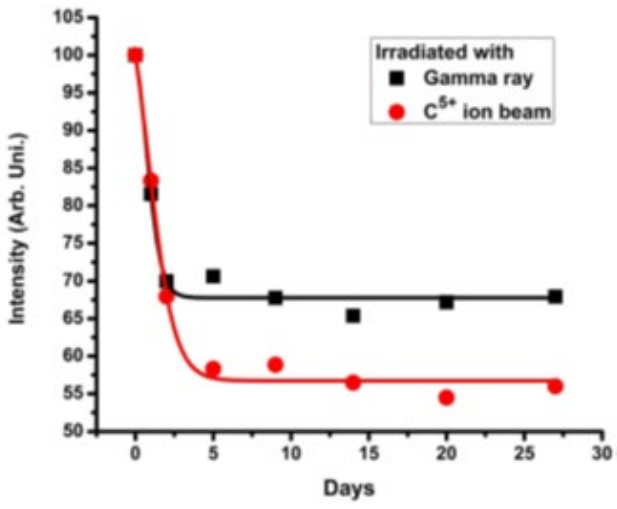

Fig. 5. Fading of synthesised $LiMgBO_3$:Dy^{3+} under exposure to γ-radiation and a C^{5+} beam according to [52]

Table 3. Kinetic parameters for $LiMeBO_3$ borates irradiated with γ-radiation

Material	Method of calculation	Peak No.	Order of kinetics	Activation energy, *E* (eV)	*S* (C^{-1})	Ref.
$LiMgBO_3:Dy^{3+}$	Форма пика	1	1.38	0.997	$1.31\cdot10^{11}$	[52]
	Вариации скоростей нагрева		1.35	1.003		
$LiMgBO_3:0.04Tb^{3+}$	Форма пика		1.1	0.92±0.01	$(1.4\pm0.2)\cdot10^{9}$	[74]
	Вариации скоростей нагрева			1.01	$1.02\cdot10^{10}$	
$LiMgBO_3:Dy^{3+}$	Форма пика	1	2	1.26	$3.09\cdot10^{16}$	[79]
		2			$3.88\cdot10^{11}$	
$LiCaBO_3:Dy^{3+}$	Форма пика	1	1.9	1.075	$2.71\cdot10^{12}$	[62]
		2	1.8	0.536	$3.173\cdot10^{5}$	
$LiCaBO_3:0.01Ce^{3+}$	Форма пика	1	2	0.655	$1.00\cdot10^{7}$	[33]
		2	1.76	1.448	$1.215\cdot10^{15}$	
		3		1.515	$7.506\cdot10^{11}$	
$LiSrBO_3$: $0.01Tm^{3+}$	Форма пика	1	1.26	0.63	$2.62\cdot10^{7}$	[101]
		2	2	0.96	$5.85\cdot10^{9}$	

for the first 3 days was approximately 30%. On the fifth day, the fading of the sample exposed to C^{+5} rays reached 42%. The $LiMgBO_3:Dy^{3+}$ sample irradiated with γ-rays showed a linear dependence of TL on the absorbed dose in the range from 10 Gy to 1 kGy. Samples irradiated with C^{+5} also showed a linear dependence of thermoluminescence on the current density in the range of $2\times^{10}$ –1×10^{11} ions/cm^2.

In [79], $LiMgBO_3:Dy^{3+}$ samples were exposed to γ-radiation of 0.01–5 kGy and fast Ag^{9+} with ion content in the range of $1\cdot10^{11}$ –$1\cdot10^{13}$ cm^{-2}. The glow curves were taken at different heating rates and were analysed by the Chen method [80]. It was found that the glow of samples exposed to ions began with a lower temperature (390 K) as compared to the glow of samples irradiated with γ-rays (396 K). The authors concluded that $LiMgBO_3:Dy^{3+}$ is suitable for γ-radiodosimetry. On the contrary, the material irradiated with heavy silver ions is not suitable for dosimetric applications, since the absorbed dose shifted even at room temperature, which leads inevitably to fading.

The thermoluminescent properties of $LiCaBO_3$ polycrystalline phosphors doped with REEs were studied in [6, 61, 82]. The $LiCaBO_3:Tm^{3+}$ samples exhibited the maximum TL sensitivity with a favourable shape of the glow curve [61]. The thermoluminescence curve of the $LiCaBO_3:Tm^{3+}$ sample irradiated with γ-rays contained 2 peaks at 230 and 430 °C, and the intensity of the second peak by almost three times exceeded the intensity of the first peak. Both peaks showed an almost linear dependence of intensity on the absorbed dose up to a value of 103 Gy. It was noted that the sensitivity of phosphor thermoluminescence to gamma radiation was about eight times higher than that ofTLD-100.

The thermoluminescence of $LiCaBO_3$ activated by dysprosium and cerium ions, when exposed to γ-quanta and a beam of C^{5+} carbon ions was studied in [62]. Both phosphors showed good TL sensitivity to the dose of γ-quanta irradiation in the range of 0.4–3.1 rad. with a ^{137}Cs source. The TL intensity increased with an increase in the content of Dy^{3+}ions in the $LiCaBO_3$ matrix and was maximum at a concentration of 0.5 mol. % Dy^{3+}. The maximum TL intensity of the second sample corresponded to the content of Ce^{3+}ions of 1 mol. %. After 20 days of exposure, the average fading for both materials was between 3 and 14%. Samples treated with a beam of C^{5+} ions showed a decrease in intensity and an increase in energy density.

In [83], thermoluminescence curves of the $LiCaBO_3:Tb^{3+}$ material contained one maximum at 240 °C and showed stability and insignificant fading.

The study of TL phosphors exposed to different types of irradiation is necessary to determine the areas of their possible use. In particular, dosimetry of heavy charged particle or heavy ion radiation is in the focus of research due to importance of its application in medicine (cancer and tumour treatment).

Searching for materials for neutron dosimetry is of paramount importance as it exhibits the highest relative biological efficiency (RBE) as compared to other types of radiation.

In [74], the method of electron paramagnetic resonance (EPR) was used to identify various defective centres caused by neutrons and gamma radiation. The lifetime of neutron-irradiated PL of materials correlated well with PL peaks and their relative contribution. To understand the kinetics of the processes, the parameters of the traps were calculated by different methods. Unlike the LiF:Mg,Ti reference, the $LiMgBO_3:Tb^{3+}$ beam thermoluminescence showed a simple glow curve. The TL sensitivity to neutrons and the ability of $LiMgBO_3:Tb^{3+}$ to separate the dose were 2.2 and 4.5 times higher than that of the standard material (Fig. 6). In addition, the TL response demonstrated excellent linearity up to a neutron dose of 105 mSv. It is noteworthy that the decay of the TL signal was < 10% when stored for 90 days. According to the diffuse reflection spectra, the green phosphor has a wide band gap (6.3 eV), is highly effective, and close to the tissue equivalent. The CIE chromaticity coordinates for $LiMgBO_3:xTb^{3+}$ phosphors are given in Table 2. According to the authors [74], the obtained characteristics meet the criteria for the practical application of the material, which can be a worthy alternative to the existing LiF:Mg,Ti dosimeter for personnel neutron dosimetry.

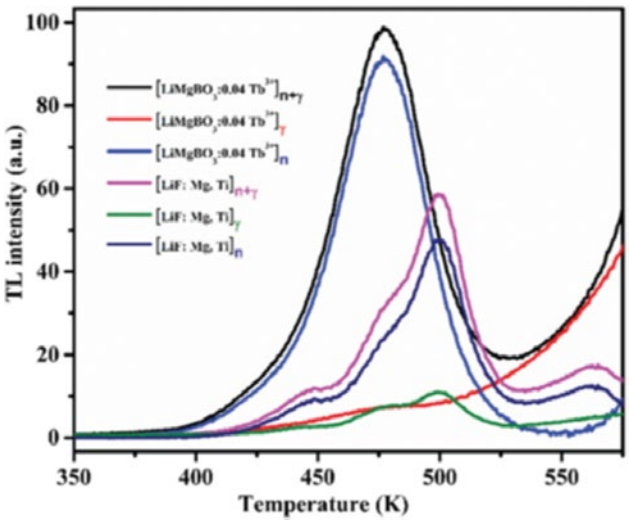

Fig. 6. Comparison of glow curves for TL $LiMgBO_3:0.04Tb^{3+}$ and LiF:Mg,Ti [74]

3.3. Upconversion (ASL, anti-stokes luminescence)

According to Stokes' rule, the photoluminescence wavelength should be greater than the excitation wavelength due to the transfer of part of the absorbed energy of the exciting light [20]. Therefore, luminescence that occurs in the visible spectrum under the influence of infrared excitation radiation is known as 'anti-stokes" luminescence. Information about anti-stokes luminescence (ASL) appeared after the study of barium fluorides doped with Er^{3+}, Ho^{3+}, Tm^{3+}, and Yb^{3+} ions [84]. In literature, it is known as upconversion, which literally means "up frequency conversion". Upconversion involves excitation and luminescence processes in systems with several energy levels. It can be observed in REE ions due to an unfilled inner *4-f* shell which is screened from the outer shells and has a unique energy structure of the levels [20, 72, 73, 85, 86]. There are three main ASL mechanisms: 1) absorption in the ground state; 2) subsequent absorption in the excited state; 3) absorption in the ground state and energy transfer to another ion. In this case, a sensitiser is the ion that gives off energy, and the ion that receives energy is known as an activator. The phenomenon of upconversion is most evident when the best initial matrix with low photon energy is chosen [20, 72, 73]. ASL formation is accompanied by the absorption of the exciting light, radiative and non-radiative processes, and the process of energy transfer.

Let us consider the processes of resonance non-radiative energy transfer and non-radiative photon transfer. Energy can be transferred from the sensitiser (S) to the activator (A) if the distance between them is quite small and the excitation energies are almost equal. In this case, A transits from the ground state to the excited state before S emits photons (Fig. 7) [86]. There is energy difference during the S → A non-radiative photon transfer so photon transfer requires the process of energy transfer to cover it. The condition for

resonance energy transfer is the overlapping of the sensitiser's radiation spectrum and the activator's absorption spectrum. Fig. 8 shows a diagram of the energy levels of Yb^{3+} and Er^{3+} ions, which explains the mechanism of luminescence sensitisation and the occurrence of glow upon excitation by IR radiation. The Yb^{3+} ion absorbs the quantum of infrared radiation in the region of 980 nm and transits to the $^2F_{5/2}$ excited state. During the resonance energy transfer to the Er^{3+} ion, it also transits to the $^2I_{11/2}$ excited state and the sensitiser returns to the $^2F_{7/2}$ ground state. After transferring the energy of the second quantum to the activator, it moves to a higher level of $^4F_{7/2}$. The $^4I_{11/2} \rightarrow {}^4F_{7/2}$ transition in the Eg^{3+} ion to the more excited state also resonates with the transition in the Yb^{3+} ion (980 nm). Having lost some of the energy in the form of photons, the excited Eg^{3+} ion first transits to the $^4S_{3/2}$ radiative level and then to the ground state emitting a quantum with an energy almost twice as much as the energy of the excitation quanta. Co-doping with Yb^{3+}- Er^{3+} ions allows obtaining blue ($^2H_{9/2} \rightarrow {}^4I_{15/2}$), green ($^2H_{11/2} \rightarrow {}^4I_{15/2}$ and $^4S_{3/2} \rightarrow {}^4I_{15/2}$), and red radiation ($^4F_{9/2} \rightarrow {}^2I_{15/2}$) [20, 87, 88], which can be explained by the considered mechanism.

There are data about the introduction of Yb^{3+} ions as an additional doping material (sensitiser) into matrices activated by Er^{3+} ions [89]. It has been reported that the luminescent properties of such materials can be improved by the resonance energy transfer from Yb^{3+} to Er^{3+} during the absorption of a photon with a wavelength of λ = 980 nm [90].

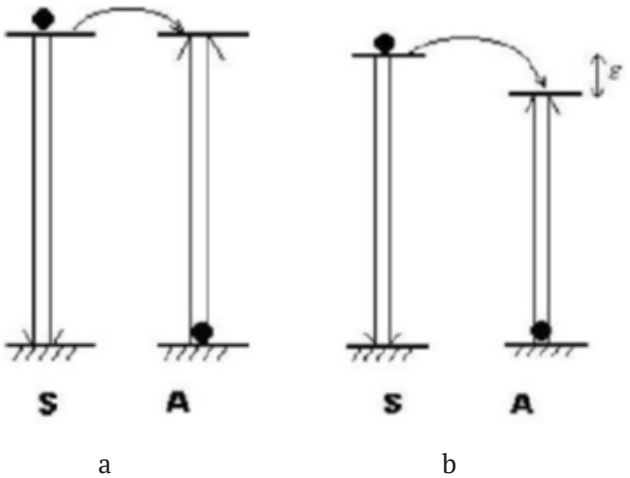

Fig. 7. Energy transfer processes between sensitiser (S) and activator (A) ions: (a) resonance non-radiative energy transfer; (b) non-radiative photon transfer [85]

Upconversion materials activated by rare earth ions are widely used in different areas starting with medicine and ending with solar energy. These are materials for solid-state lasers, biological sensors, laser beam visualisers, solar batteries, etc [86–91].

The phenomenon of upconversion in the $LiMgBO_3$ samples with a fixed concentration of Er^{3+} and Yb^{3+} ions has been studied [65]. The absorption spectrum of the $LiMgBO_3$:0.02 Er^{3+}, 0.08 Yb^{3+} phase showed a wide band with a maximum intensity in the region of 820–1,080 nm at λ = 980 nm ($^4I_{15/2} \rightarrow {}^4I_{11/2}$ resonance transitions in Er^{3+} and $^2F_{7/2} \rightarrow {}^2F_{11/2}$ resonance transitions in Yb^{3+}). There were also two peaks with wavelengths of 545 and 656 nm, which corresponded to the $^4I_{15/2} \rightarrow {}^4S_{3/2}$ and $^4I_{15/2} \rightarrow {}^4F_{9/2}$ transitions in Er^{3+} ions. The upconversion spectra of the phosphor showed Er^{3+} emission in the range (590 and 596 nm) due to mixed transitions from $^4F_{9/2}$ and $^4S_{3/2}$ to $^4I_{15/2}$. Works [92, 93] studied the upconversion emission properties of $LiBaBO_3$ and

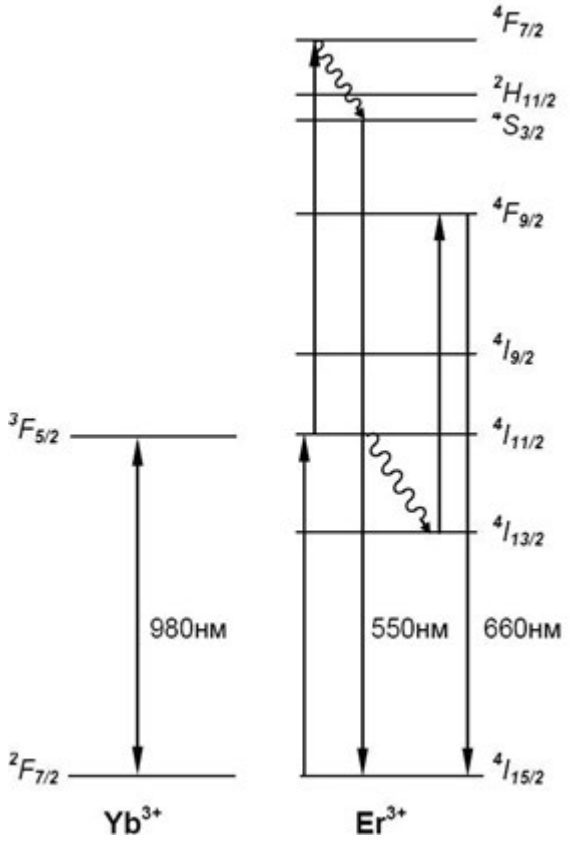

Fig. 8. Diagram of the energy levels of Yb^{3+} and Er^{3+} ions [20]

$LiSrBO_3$ borates doped with Er^{3+} and Yb^{3+} ions with fixed concentrations. The synthesised materials emitted light in the visible region after excitation in the infrared region. $LiBaBO_3$:0.02Er^{3+}, 0.08Yb^{3+} and $LiSrBO_3$:0.02Er^{3+}, 0.08Yb^{3+} phosphors showed absorption lines in the infrared region, 820-1,080 nm and at 545 nm, 656 nm, respectively. The upconversion spectra of phosphors showed persistent emission in Er^{3+} ions (590 and 596 nm) due to mixed transitions from $^4F_{9/2}$ and $^4S_{3/2}$ to $^4I_{15/2}$. Intense radiation with increasing frequency in these crystal phosphors can be useful in various areas of modern lighting technology.

To adjust the colours or increase the radiation intensity, heavy metal ions, for example, Mn^{2+}, Bi^{3+}, can be doped together with REE ions [25, 94]. Bi^{3+} ions as a co-activator can act as a primary energy excitation centre and non-radiatively transfer their energy to enhance the radiation intensity of another dopant ion, i.e. play the role of a sensitiser [63].

The tunable luminescence of a number of $LiBaBO_3$:Ce^{3+}/Mn^{2+} samples was studied by Li et al. [34]. The authors expected the $Ce^{3+}\rightarrow Mn^{2+}$ energy transfer due to the overlapping $LiBaBO_3$:Ce^{3+} emission spectrum and the $LiBaBO_3$:Mn^{2+} absorption spectrum. It was confirmed that the process of the $Ce^{3+}\rightarrow Ce^{3+}$ non-radiative energy transfer can be described by exchange interaction, radiation reabsorption, and multipolar interaction. When the content of Ce^{3+} ions was 5 mol.%, the glow intensity of borates gradually decreased with an increase in the concentration of Mn^{2+} ions, which can be explained by an increase in the efficiency of the $Ce^{3+}\rightarrow Mn^{2+}$ energy transfer. The glow colour of the $LiBaBO_3$:5 mol. % Ce^{3+}/y mol. % Mn^{2+} phosphors (y = 0, 1, 2, 3, 4, and 5) changed from blue to orange. It was noted that the material with the composition of $LiBaBO_3$:5 mol. % Ce^{3+}/2 mol. % Mn^{2+} had a glow close to white light. Previously, double blue and orange radiation, which is the result of 5*d*–4*f* transitions in Ce^{3+} ions and a forbidden transition in Mn^{2+} ions, was detected in $LiCaBO_3$:Ce^{3+}, Mn^{2+} [94]. The process of the $Ce^{3+}\rightarrow Mn^{2+}$ energy transfer was classified as resonance transfer. It has a dipole-dipole (*d*-*d*) mechanism with a critical distance of about 4.1 Å. Due to strong excitation bands in the range of 325–375 nm, the studied phosphors with double radiation can be used in near UV radiation light-emitting diodes (LEDs). The same energy transfer mechanism has been found in $LiSrBO_3$:Ce^{3+}, Tb^3 polycrystals [95].

The photoluminescent, structural, and optical properties of $LiBaBO_3$ phosphors doped with Eu^{3+} ions and codoped with Bi^{3+} ions were studied by Lephoto and colleagues [7]. They studied the mechanism of the $Bi^{3+}\rightarrow Eu^{3+}$ energy transfer. The materials showed tunable radiation based on simultaneous broadband radiation at a wavelength of 593 nm and narrowband radiation associated with the *f*–*d* and *f*–*f* Eu^{2+} and Eu^{3+} transitions, respectively. According to the results of the study, part of Eu^{3+} ions reduced to Eu^{2+}. The samples had greenish-blue (493 nm) and red (613 nm) glows, which were attributed to the emission of Eu^{2+} and Eu^{3+} ions. Co-alloying with Bi^{3+} ions significantly increased the intensity of the Eu^{3+}narrowband radiation, whose maximum was located at a wavelength of 613 nm. Narrowband radiation at 613 nm depended on the concentration of the co-activator, which indicated a non-radiative transfer of energy from Bi^{3+} ions to Eu^{3+} ions. Chromatic coordinates according to (CIE) are given in Table 2.

3.4. Photoluminescent properties

$LiCaBO_3$

Excitation and emission spectra of $LiCaBO_3$:Tb^{3+} materials were studied in [6, 14, 53, 83]. A study of the effect of embedded ions (Li^+, Na^+, K^+) on the emission intensity of $LiCaBO_3$:Tb^{3+} showed that it is maximum for Li^+ ions (4 mol. %) [14]. The results [14] are consistent with the data presented in work [83], in which the maximum green emission of $LiCaBO_3$:Tb^{3+} was observed at a wavelength of 545 nm. At UV excitation with λ_{em} = 254 nm, 4 distinct bands at wavelengths of 486, 545, 590, and 622 nm were detected in the emission spectrum corresponding to typical radiative transitions of Tb^{3+} ions: $^5D_4\rightarrow{}^7F_6$, $^5D_4\rightarrow{}^7F_5$, $^5D_4\rightarrow{}^7F_4$, $^5D_4\rightarrow{}^7F_3$. Among the emission lines, the dominant emission was observed at 547 nm, which corresponded to the $^5D_4\rightarrow{}^7F_5$ transition. The $^5D_4\rightarrow{}^7F_5$ emission line is the strongest line in almost all crystalline matrices when the Tb^{3+} content is a few mole percent or higher [53]. Photoluminescence radiation and excitation spectra were studied in detail for

$LiCa_{1-x}BO_3$:$x$$Tb^{3+}$ with x = 0.005. The excitation spectrum at λ_{em} = 547 nm had a wide band in the range of 250–300 nm, which corresponded to the $f^8 \rightarrow 4\ f^7 5d$ permitted transitions of Tb^{3+} ions. In [14], the emission intensity increased with increasing concentration of active ions and reached a maximum at 3 mol. % Tb^{3+}. The authors [6] associated this with the greatest probability of attributing these transitions to both electric dipole and magnetic dipole induced transitions.

According to the authors [53], the peak at ~240 nm in the excitation spectra can be easily classified as $4f^8–4f^7 5d$ spin permitted transitions of Tb^{3+}, whose exact position depends on the crystalline field of the lattice. For λ_{ex} = 240 nm, the radiation intensity first increased with increasing activator concentration and reached a maximum at x = 0.005. After that, there was a concentration quenching mainly associated with the quadrupole-quadrupole interaction. The CIE chromaticity coordinates for the synthesised green $LiCaBO_3$:Tb^{3+} phosphor are given in Table 2.

According to the excitation and emission spectra data, $LiCaBO_3$:Eu^{3+} phosphors were excited effectively by near UV (400 nm) and blue light (470 nm) and emitted red light [13]. The radiation intensity increased with increasing concentration of Eu^{3+} and reached a maximum at 3 mol. % Eu^{3+}. Then, the intensity decreased due to concentration quenching. According to Dexter's theory [96], the mechanism of concentration quenching of Eu^{3+} ions in $LiCaBO_3$ is caused by a dipole-dipole interaction. In [97], $LiCaBO_3$:Dy^{3+}/Eu^{3+} phosphors were characterised by photoluminescence spectra. $LiCaBO_3$:Dy^{3+} emission spectra showed two peaks (484 and 577 nm). The maximum radiation intensity was shown by the $LiCaBO_3$: 0.01Dy^{3+} sample. A further increase in the activator content led to concentration quenching and the calculated critical distance between the Dy^{3+} ions was about 22.76 Å. Similar to [13], the red radiating $LiCaBO_3$:Eu^{3+} phosphor can be excited effectively by near UV radiation (392 nm). The emission spectra showed the $^5D_0 \rightarrow {}^7F_J$ (J = 0–2) transition with the main glow at a wavelength of 614 nm due to the electric-dipole transition caused by an acentric point group. The $LiCaBO_3$:Eu^{3+} sample had concentration quenching at 0.2 mol. % and the critical distance was about 38.93 Å. The critical distance was defined as the average distance between the closest Eu^{3+} ions involved in the energy transfer. According to Dexter's theory, the concentration quenching of inorganic materials is determined by electric multipolar interaction or magnetic dipole interaction between activator ions. The authors associated concentration quenching of the $LiCaBO_3$:Eu^{3+} phosphor with non-radiative transitions between Eu^{3+} ions.

$LiCaBO_3$:Dy^{3+} photoluminescence temperature dependence was studied by Beck et al. [98] The time of luminescence emission and decay were recorded in the temperature range of 100–480 K. It was found that the maximum intensity of PL radiation was observed when the content of active Dy^{3+} ions was 2–3 mol. %. The emission intensity ratios (Y/B) were selected depending on the concentration of Dy^{3+} ions. The $LiCaBO_3$:Dy^{3+} material had excellent heat resistance, its colour was in the near white region, the values of the correlated first and total temperature were in the range of 4,955–5,955 K. It was found that the phosphor's quantum yield was 0.25 and the width of the band gap was 4.85 eV. The photoluminescent properties of $LiCaBO_3$ borates doped with different concentrations of Pb^{2+} and Bi^{3+} ions were studied at room temperature [99]. $LiCaBO_3$:Pb^{2+} and $LiCaBO_3$:Bi^{3+} radiation emission bands were observed at wavelengths of 296 nm and 378 nm, respectively. The calculated Stokes shifts of the samples was 3,952 nm^{-1} for $LiCaBO_3$:Pb^{2+} and 6,440 nm for $LiCaBO_3$:Bi^{3+}.

$LiCaBO_3$:Gd^{3+} phosphors have been characterised by photoluminescence spectroscopy and electron paramagnetic resonance (EPR) [100]. The introduction of the Gd^{3+} ion into the $LiCaBO_3$ matrix lattice contributed to the appearance of a narrow band of UV radiation at a wavelength of 315 nm when excited with λ = 274 nm. The mechanism of concentration quenching was studied and described.

$LiSrBO_3$

The luminescent characteristics of $LiSrBO_3$ activated by REE ions was studied in works [28, 29, 32, 101]. Excitation and emission spectra for $LiSrBO_3$:M, M = Ce^{3+}, Eu^{2+}, Eu^{3+}, Sm^{3+}, Tb^{3+}, Dy^{3+} showed effective excitation with UV LEDs and satisfactory red, green, and blue characteristics [28].

The authors [29] compared their results with the data [102] and discovered a difference in the location of the photoluminescence excitation bands (PLE) and photoluminescence, as well as the difference in the energies of the higher and lower energy levels. They attributed the differences to the different crystallinities of the samples, greater bond covalence, and the high crystal field splitting. The results of the prefabricated LED are shown in Fig. 9. The experimental sample of the material was produced by combining a 460 nm LED chip with $LiSrBO_3:Eu^{2+}$ borate. The quantum efficiency of the $LiSrBO_3:Eu^{2+}$ material was significantly inferior to the quantum efficiency of the commercial red phosphor (18% of the industrial phosphor). The authors concluded that it is necessary to optimise the content of Eu^{2+}, its crystallinity and to increase its quantum efficiency to use the new $LiSrBO_3:Eu^{2+}$ material.

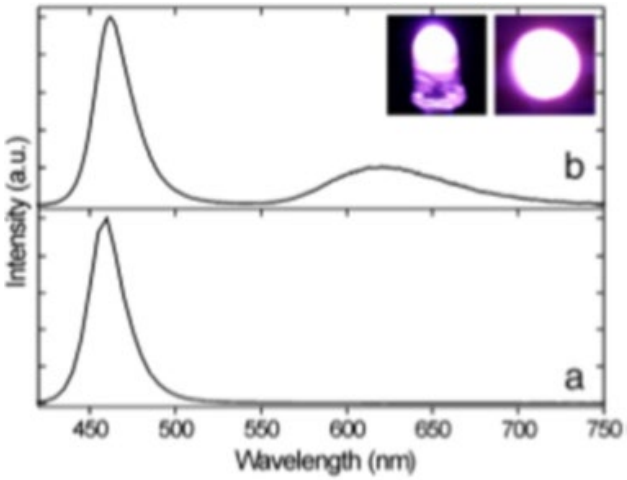

Fig. 9. Emission spectra of (a) a 460 nm bare chip LED and (b) a 460 nm LED chip combined with sample B [29]

The emission band of trivalent thulium ions with a centre at about 450 nm coincided with one of the absorption bands of dysprosium ions [103, 104]. Therefore, energy transfer is possible between Dy^{3+} and Tm^{3+} ions in the same matrix. Tm^{3+} ions can be added as a sensitiser to increase the luminescence intensity of powders doped with Dy^{3+}. $LiSrBO_3$ borates were co-doped with Dy^{3+}, Tm^{3+}, and Eu^{3+} in [32]. According to powder X-ray data, active REE ions completely dissolved in the host lattice and occupied positions that did not coincide with the inversion centre. According to the excitation spectra data, phosphors were effectively excited by UV at 350–400 nm. At a doping concentration of $x = 0.03$, there was concentration quenching of $LiSrBO_3:Na^+$, Tm^{3+}. The lifetime of $LiSrBO_3:0.05Dy^{3+}$, $0.005Tm^{3+}$; $LiSrBO_3:0.01Dy^{3+}$, $0.005Tm^{3+}$, and $LiSrBO_3:0.015Dy^{3+}$, $0.005Tm^{3+}$ phosphors calculated from the decay curves was 0.99 ms, 0.986 ms, and 0.96 ms, respectively. Compositional dependence of the luminescence properties were studied for the $LiSrBO_3:x(Tm^{3+},$

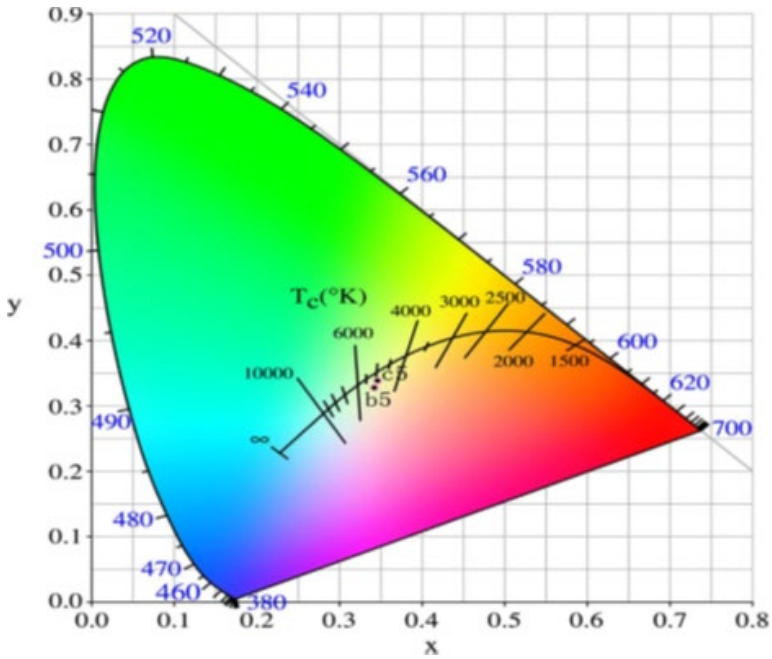

Fig. 10. Correlated colour temperature chart for $LSBO:0.01Dy^{3+}$, $0.005Tm^{3+}$, $0.03Eu^{3+}$, and $LSBO:0.015Dy^{3+}$, $0.005Tm^{3+}$, $0.03Eu^{3+}$ exited at 380 nm [32]

Na^+) samples. According to the chromaticity diagrams, phosphors can emit white light: from cold to warm (see Fig. 10).

In [8], when $LiSrBO_3:Sm^{3+}$ borate was exposed to UV radiation (221 nm) and a low-voltage electron beam (2 keV, 12 mA/cm^2), there was a strong emission at a wavelength of 601 nm corresponding to the $^4G_{5/2}\rightarrow H_{7/2}$ transitions of Sm^{3+} ions. Prolonged bombardment with low-energy electrons resulted in stable emission of cathodoluminescence (CL), which appeared after a dose of electrons of 100 CL/cm^2. Before and after a dose of electrons of 300 Kl/cm^2, the shape of the emission spectra of Auger electrons changed and their energy shifted for boron and strontium atoms in the structure of the $LiSrBO_3:Sm^{3+}$ material. It was assumed that during bombardment with an electron beam new surface chemicals formed which were responsible for the cathodoluminescence stability in the new orange-red phosphor.

$LiBaBO_3$

The analysis of the $LiBaBO_3:Sm^{3+}$ excitation and emission spectra showed that the material is excited effectively by ultraviolet (UV) light and demonstrates satisfactory red light characteristics (597 nm), which makes it fit easily into the UV LED chip [105]. The radiation intensity of the $LiBaBO_3:Sm^{3+}$ phosphor increases with an increase in the content of Sm^{3+} ions up to 3 mol. % followed by concentration quenching. The quenching mechanism is associated with the *d–d* interaction according to Dexter's theory. The glow intensity of the materials increases due to compensation of the charge of the doping alkaline Li^+, Na^+, K^+ ions. What is more, it is higher when doped with Li^+ ions as compared to Na^+ and K^+ ions [105, 13, 14, 28].

Meng et al [106] investigated optical properties of $LiBaBO_3$ borate doped with Eu^{2+} at a temperature between 10 and 525 K. The excitation spectra contained wide bands at wavelengths from 220 to 450 nm. The wide emission band with a maximum of about 485 nm observed at room temperature was attributed to the $4f^65d^1\rightarrow 4f^7$ transition of Eu^{2+} ions. The radiation intensity decreased insignificantly at temperatures below room temperature, however, it dropped sharply at higher temperatures. The calculated Stokes shift was 0.52 eV.

$LiZnBO_3$

Wang and collaborators [48] investigated α-$LiZnBO_3:Mn^{2+}$ borate. They expected substitution of Zn^{2+} ions with Mn^{2+} ions in the tetrahedron. The presence of Mn^{2+} ions in the α-$LiZnBO_3$ matrix was confirmed by EPR spectra. Strong narrow absorption bands in the range of 400–450 nm were found in the light reflection spectra of all doped samples. During excitation with a wavelength of 431 nm, there was an abnormal red emission band in the range of 550–800 nm due to a strong crystalline field caused by a distorted tetrahedron. The emission spectra contained a wide band of red radiation with a maximum at 647 nm for all doped samples regardless of the excitation wavelength and Mn^{2+} concentration. Red radiation is anomalous for the tetrahedral-coordinated Mn^{2+} in α-$LiZnBO_3$. The authors associated it with further splitting of the *d*-level of Mn^{2+} during the $^4T_1\,(^4G)\rightarrow{}^6A_1\,(^6S)$ transition from the excited state to the ground state. At a concentration of x = 7 mol. % Mn^{2+} luminescence quenching was observed. The calculated phosphor chromaticity coordinate (0.66, 0.34) was very close to the standard red colour (0.66, 0.33).

The optical properties of the orange-red $LiZnBO_3:Sm^{3+}$ phosphor obtained by solution combustion were investigated by photoluminescence and ultraviolet-visible spectroscopy [107]. In the radiation spectrum at λ_{ex} = 401 nm, there were peaks at 565, 602, and 648 nm, which were attributed to electric dipole transitions. The width of the material's band gap calculated from the diffuse reflection spectrum was 5.8 eV. It was concluded that it is possible to use this phosphor in near UV LEDs.

4. Conclusions

The analysis of the literature dedicated to the production of $LiMeBO_3$ borates (Me = Mg, Ca, Sr, Ba, Zn, Cd) revealed a variety of possible methods of their synthesis. Polycrystalline borates are traditionally obtained by high-temperature solid-phase reactions. The starting materials are the corresponding nitrates or carbonates. Sometimes a reducing atmosphere is used to dope samples with REE ions to avoid possible oxidation of ions with variable valence at high temperatures. Along with the traditional solid-phase method, such methods as SHS and its modifications

have become widespread. These relatively new methods based on the combustion reaction, require reagents that promote the self-sustaining exothermic reaction. Normally, these are such accessible materials as urea and ammonium nitrate used as fuel and oxidiser. They allow obtaining nanoscale powders. $LiMeBO_3$ lithium and alkaline earth metal borates are successfully doped with rare earth ions (Ce^{3+}, Sm^{3+}, Gd^{3+}, Eu^{2+}, Eu^{3+}, Tb^{3+}, Dy^{3+}, Tm^{3+}, Er^{3+}, Yb^{3+}) and Mn^{2+}, Pb^{2+}, Bi^{3+} heavy metal ions. Co-doping is also used, for example, REE ions –REE: Dy^{3+} with Eu^{3+}; Dy^{3+} with Tm^{3+}; Ce^{3+} with Tb^{3+} and Er^{3+} with Yb^{3+} or REE ions – Me^{2+} or REE-M^{3+}, for example, Ce^{3+}/Mn^{2+}; Eu^{3+}/Bi^{3+}. Some works provide information about the size, morphology, microstructure of particles and attempt to analyse the effect of codoping on the morphology of particles. For example, in [25] it was noted that doping with Bi^{3+} ions affects the morphology of $LiMgBO_3:Eu^{3+}$. According to SEM of the $LiMg_{0.945}BO_3:Eu^{3+}_{0.05},Bi^{3+}_{0.005}$ borate, the size of phosphor particles increases with the addition of Bi^{3+} ions. Table 4 presents data on synthesis methods and possible areas of application of some representatives of the studied borates.

Literature indicates the possibility to use $LiMeBO_3$ borate compounds to develop luminescent matrices. These are framework crystalline structures. They are based on polyhedra of large metals linked by common edges and vertices of boron-oxygen triangles that are not connected to each other. Numerous spectral luminescence studies which have been carried out in recent decades have shown their ability to emit light after the absorption of external energy (UV, X-rays, γ-radiation, etc.). The spectral data considered in this paper were obtained by methods of photoluminescence analysis, thermoluminescence, upconversion, etc. It is known that external influences affect the structure of the material and leads to its defectiveness. The introduction of dopants into the crystalline structure also causes its distortion. For example, the introduction of rare earth elements creates a new energy of state near the conduction band that alters this phenomenon. The excellent luminescent properties of ions of rare-earth elements arise from the possibility of electronic transitions between states within the 4*f*-configuration. This becomes possible because the ground state configurations are always half full, the 4*f* shell is screened by the 5*s* and 5*p* outer electron shells. Doped activator ions often become the main part of the phosphor luminescence centre. Sometimes the activator ion exhibits low absorption and another ion (sensitiser) is added to start the luminescence process [25, 32, 34, 62, 94, 95]. The absorbed energy is transferred from the sensitiser to the activator. After that, the activator emits a photon of a certain wavelength. Small

Table 4. Methods of synthesis and possibilities of $LiMeBO_3$ application

Matrix	Doping ions	Method of synthesis	Area of possible	Reference
$LiMgBO_3$	Eu^{3+}, Bi^{3+}	Solid-phase	White LEDs	[25]
$LiMgBO_3$	Dy^{3+}	Solution combustion	Dosimetry	[50]
$LiMgBO_3$	Er^{3+}/ Yb^{3+}	Solution combustion	Phosphor	[65]
$LiCaBO_3$	Eu^{3+}	Solid-phase	Red phosphor for white LEDs	[13]
$LiCaBO_3$	Tb^{3+}	Solid-phase	Green phosphor for white LEDs	[14]
$LiCaBO_3$	Dy^{3+}	Solid-phase	White LEDs	[98]
$LiSrBO_3$	Eu^{3+}, Sm^{3+},Tb^{3+} Ce^{3+}, Dy^{3+}	Solid-phase	Red phosphor for white LEDs	[28]
$LiSrBO_3$	Eu^{2+}	Solid-phase	Yellow phosphor for white LEDs	[29]
$LiSrBO_3$	Dy^{3+}, Tb^{3+}, Tm^{3+}, Ce^{3+}	Solid-phase	Dosimetry	[101]
$LiBaBO_3$	Ce^{3+}/ Mn^{2+}	Solid-phase	White LEDs	[34]
α-$LiZnBO_3$	Mn^{2+}	Solid-phase	Red phosphor	[48]
$LiZnBO_3$	Sm^{3+}	Solution combustion	White LEDs	[107]
α-$LiCdBO_3$		Solid-phase	Pink phosphor	[36]
β-$LiCdBO_3$		Solid-phase	Red phosphor	[36]

amounts of dopants cause minor defects in the $LiMeBO_3$ structure leading to blue, green, and red light emissions of great commercial interest. The introduction of a suitable dopant may improve the luminescent properties of these borates. When bivalent Me^{2+} ions are substituted in $LiMeBO_3$ with trivalent ions, such as Tb^{3+}, Eu^{3+}, the balance of charges is disturbed. Compensation is possible by introducing into the ions' structure Li^+, Na +, K^+ alkali metals affecting the emission yield. In all considered cases, the radiation intensity increased. It was shown experimentally that the most suitable charge compensator is Li^+ ions.

Some crystals are capable of self-producing luminescence under certain conditions. For example, in UV light $LiCdBO_3$ crystals of the triclinic modification produce red luminescence and in IR light they produce yellow luminescence [36]. Co-doping of REE ions (Ce^{3+}, Eu^{3+}) with heavy metal ions, such as Mn^{2+}, Bi^{3+}, in $LiMeBO_3$ contributes to an increase in the radiation intensity in the materials and allows tuning colours from blue to orange.

Numerous studies dedicated to the conditions for obtaining $LiMeBO_3$ borates, methods of their synthesis, and their spectral-luminescent properties allow considering them as promising materials. They can be considered as phosphors that emit green, blue, and red light, which can be used in white LEDs and as effective materials for personnel neutron dosimetry and the dosimetry of weak ionising radiation.

Conflict of interests

The author declares that they has no known competing financial interests or personal relationships that could have influenced the work reported in this paper.

References

1. Nakamura S., Fasol G. *The Blue Laser Diode*. Berlin: Springer, 1997. p. 343. https://doi.org/10.1007/978-3-662-03462-0

2. Cho J., Park J. H., Kim J. K., Schubert E. F. White light-emitting diodes: History, progress, and future. *Laser & Photonics Reviews*. 2017;11(2): 1600147. https://doi.org/10.1002/lpor.201600147

3. Zheng J., Cheng Q., Wu J., Cui X., Chen R., Chen W., Chen C. A novel single-phase white phosphor: Dy^{3+}, K^+ for near-UV white light-emitting diodes. *Materials Research Bulletin*. 2016;73: 38–47. https://doi.org/10.1016/j.materresbull.2015.08.007

4. Zhu G., Wang Y., Wang Q., Ding X., Geng W., Shi Y. A novel white emitting phosphor of Dy^{3+} doped $Ca_{19}Mg_2(PO_4)_{14}$ for light-emitting diodes. *Journal of Luminescence*. 2014;154: 246–250. https://doi.org/10.1016/j.jlumin.2014.04.041

5. Ji Y., Cao J., Zhu Z., Li J., Wang Y., Tu C. Synthesis and white light emission of Dy^{3+} ions doped hexagonal structure $YAlO_3$ nanocrystalline. *Journal of Luminescence*. 2012;132: 702–706. https://doi.org/10.1016/j.jlumin.2011.10.019

6. Bajaj N. S., Omanwar S. K. Combustion synthesis and thermo luminescence in γ-irradiated borate phosphors activated with terbium (III). *Asian Journal of Chemistry*. 2012;24: 5945–5946.

7. Lephoto M. A., Tshabalala K. G., Motloung S. J., Shaat S. K. K., Ntwaeaborwa O. M. Tunable emission from $LiBaBO_3$: Eu^{3+}; Bi^{3+} phosphor for solid-state lighting. *Journal of Luminescence*. 2017;32(6): 1084–1091. https://doi.org/10.1002/bio.3295

8. Pitale S. S., Nagpure I. M., Kumar V., Ntwaeaborwa O. M., Terblans J. J., Swart H. C. Investigations on the low voltage cathodoluminescence stability and surfacechemical behaviour using Auger and X-ray photoelectron spectroscopy on $LiSrBO_3$:Sm^{3+}phosphor. *Materials Research Bulletin*. 2011;46: 987–994. https://doi.org/10.1016/j.materresbull.2011.03.022

9. Raghuvanshi G. S., Bist H. D., Kandpal H. C. Luminescence characteristics of Dy^{3+} in different host matrices. *Journal of Physics and Chemistry of Solids*. 1982;43(8): 781–783. https://doi.org/10.1016/0022-3697(82)90246-3

10. Huy B. T., Quang V. X., Chau H. T. B. Effect of doping on the luminescence properties of $Li_2B_4O_7$. *Journal of Luminescence*. 2008;128: 1601–1605. https://doi.org/10.1016/j.jlumin.2008.03.007

11. Bubnova R., Volkov S., Albert B., Filatov S. Borates-crystal structures of prospective nonlinear optical materials: high anisotropy of the thermal expansion caused by anharmonic atomic vibrations. *Crystals*. 2017;7: 93. https://doi.org/10.3390/cryst7030093

12. Li P., Yang Z., Wang Z., Guo Q. Luminescent characteristics of $LiCaBO_3$:Eu^{3+} phosphor for white light emitting diode. *Journal of Rare Earths*. 2009; 27(3): 390–393. https://doi.org/10.1016/S1002-0721(08)60257-4

13. Wang Z., Yang Z., Li P., Guo Q., Yang Y. Luminescence characteristic of $LiCaBO_3$: Tb^{3+} phosphor for white LEDs. *Journal of Rare Earths*. 2010;28(1): 30–33. https://doi.org/10.1016/S1002-0721(09)60044-2

14. Un A. Investigation of dopant effect on some TL dosimeters containing boron. *Radiation Physics and Chemistry*. 2013;85: 23–35. https://doi.org/10.1016/j.radphyschem.2012.10.016

15. Omanwar S. K., Koparkar K. A., Virk H. S. Resent advances and opportunites in TLD materials: a review.

Defect and Diffusion Forum. 2014;347: 75–110. https://doi.org/10.4028/www.scientific.net/DDF.347.75

16. Chikte D., Omanwar S. K. Moharil S. V. Luminescence properties of red emitting phosphor $NaSrBO_3:Eu^{3+}$ prepared with novel combustion synthesis method. *Journal of Luminescence*. 2013;142: 180–183. https://doi.org/10.1016/j.jlumin.2013.03.045

17. Doull B. A., Oliveira L. C., Wang D. Y, Milliken E. D., Yukiharan E. G. Thermoluminescent properties of lithium borate, magnesium borate and calcium sulfate eveloped for temperature sensing. *Journal of Luminescence*. 2014;146: 408–417. https://doi.org/10.1016/j.jlumin.2013.10.02218

18. Verma S., Verma K., … Swart H. C. Recent advances in rare earth doped alkali-alkaline earth borates for state lighting applications. *Physica B: Condensed Matter*. 2018;535: 106–113. https://doi.org/10.1016/j.physb.2017.06.07319

19. Lakshmanan A. R. A review on the role of thermoluminescent dosimeters in fast-neutron personnel dosimetry. *Nuclear Tracks and Radiation Measurements*. 1982;6(2–3): 59–78. https://doi.org/10.1016/0735-245X(82)90030-8

20. Petrik V. I. *Anti-Stokes compounds and materials based on them**. Irkutsk: Oblastnaya tipografiya No 1 Publ., 2012. 400 p. (In Russ.)

21. Budzanowski M., Bilski P., Olko P., Niewiadomski T., Burgkhardt B., Piesch E. New TL detectors for personal neutron dosimetry. *Radiation Protection Dosimetry*. 1993;47(1-4): 419–423. https://doi.org/10.1093/rpd/47.1-4.419

22. Horowitz Y. S. LiF:Mg,Ti versus LiF:Mg,Cu,P: the competition heats up. *Radiation Protection Dosimetry*. 1993;47(1-4): 135–141. https://doi.org/10.1093/oxfordjournals.rpd.a081718

23. Lee J. I., Yang J. S., Kim J. L., Pradhan A. S., Lee J. D., Chung K. S., Choe H. S. Dosimetric characteristics of LiF:Mg,Cu,Si thermoluminescent materials. *Applied Physics Letters*. 2006; 89: 094110. https://doi.org/10.1063/1.234528024

24. Subanakov A. K., Bazarov B. G., Perevalov A. V., Bazarova Zh. G. Thermoluminescent phosphor synthesis on the basis of MgB_4O_7:Dy. *Advances in Current Natural Sciences*. 2016;12(2): 36–41. (In Russ.). Available at: https://natural-sciences.ru/ru/article/view?id=36257

25. Liang Z., Mo F., Zhang X., Zhoun L. Luminescence of the $LiMgBO_3:Eu^{3+}$, Bi^{3+} phosphor. *Journal of Luminescence*. 2014; 151:47–51. http://dx.doi.org/10.1016/j.jlumin.2014.02.001

26. Wu L., Chen X. L., Tu Q. Y., He M., Zhang Y., Xu Y. P. Phase relations in the system Li_2O-MgO-B_2O_3. *Journal of Alloys and Compounds*. 2002;33391-2): 154-158. https://doi.org/10.1016/S0925-8388(01)01702-9

27. Bazarova Zh. G., Nepomnyashchikh A. I., Kozlov A. A., … Kurbatov R. V. Phase equilibria in the Li_2O–MgO–B_2O_3 system. *Russian Journal of Inorganic Chemistry*. 2007;52: 1971–1973. https://doi.org/10.1134/S003602360712025X

28. Li P., Wang Z., Yang Z., Guo Q., Fu G. Luminescent characteristics of $LiSrBO_3$:M (M= Eu^{3+}, Sm^{3+}, Tb^{3+}, Ce^{3+}, Dy^{3+}) phosphor for white light-emitting diode. *Materials Research Bulletin*. 2009;44: 2068–2071. https://doi.org/10.1016/j.materresbull.2009.07.008

29. Zhang J., Zhang X., Gong M., Shi J., Yu L., Rong C., Lian S. $LiSrBO_3:Eu^{2+}$: A novel broad-band red phosphor under the excitation of a blue light. *Materials Letters*. 2012;79: 100–102. https://doi.org/10.1016/j.matlet.2012.04.011

30. Cheng W.-D., Zhang H., Lin Q.-S., Zheng F.-K. Syntheses, crystal and elektronic structures and linear optics of $LiMBO_3$ (M = Sr, Ba) orthoborates. *Chemistry of Materials*. 2001;13: 1841–1847. https://doi.org/10.1021/cm000808i

31. Wu L., Chen X. L., Li H., He M., Dai L., Li X. Z., Xu Y. P. Structure determination of a new $LiCaBO_3$. *Journal of Solid State Chemistry*. 2004;177: 1111–1116. https://doi.org/10.1016/j.jssc.2003.10.018

32. Cai G. M., Yang M., Liu H. X., Si J. Y., Zhang Y. Q. Single-phased and color tunable $LiSrBO_3:Dy^{3+}$, Tm^{3+}, Eu^{3+} phosphors for white-light-emitting application. *Journal of Luminescence*. 2017;187: 211–220. https://doi.org/10.1016/j.jlumin.2017.03.017

33. Jiang L. H., Zhang Y. L., Li C. Y., Pang R., Hao J. Q., Su Q. Thermoluminescence characteristics of rare-earth-doped $LiCaBO_3$ phosphor. *Journal of Luminescence*. 2008;128: 1904–1908. https://doi.org/10.1016/j.jlumin.2008.05.017

34. Li J., Li X., Xing H.-W., Zhang Y.-Z., Yang A.-M., Pan Y.-H., Liu W.-X. Solid state synthesis of $LiBaBO_3:Ce^{3+}/Mn^{2+}$ Phosphors and tunable luminescence induced by energy transfer from Ce^{3+} to Mn^{2+}. *Journal of Materials Science – Materials in Electronics*. 2017;28: 4738–4743. https://doi.org/10.1007/s10854-016-6117-6

35. Lehmann H.-A., Schadov H. Bildung und darstellung von gemischten monoboraten des typs $MeLiBO_3$, (Me = Co, Zn, Mn). *Zeitschrift für Anorganische und Allgemeine Chemie*. 1966;348: 42-48. https://doi.org/10.1002/zaac.19663480106

36. Buludov N. T., Karaev Z. Sh., Abdullaev G. K. $LiBO_2$–CdO system. *Russian Journal of Inorganic Chemistry*. 1985;30(6): 1523–1526. (In Russ.).

37. Wei L., Huang Q., Zhou Z., Yin X., Dai G., Liang J. Phase diagram of the $LiBO_2$–CdO system, phase transition, and structure of $LiCdBO_3$. *Journal of Solid State Chemistry*. 1990; 89(1): 16–22. https://doi.org/10.1016/0022-4596(90)90289-A

38. Yin X. D., Huang Q. Z., Ye S. S., Lei S. R., Chen C. T. Search for the borate nonlinear optical materials: synthesis of lithium cadmium borate α-$LiCdBO_3$. *Acta Chimica Sinica*. 1985;43(9): 822–826. Available at:

http://sioc-journal.cn/Jwk_hxxb/EN/Y1985/V43/I9/822

39. Khamaganova T. N., Khumaeva T. G. Phase Equilibria in the $Li_2O–CdO–B_2O_3$ system. *Russian Journal of Inorganic Chemistry*. 2013;58(12): 1571–1575. https://doi.org/10.1134/s0036023614010057

40. Khamaganova T. N., Khumaeva T. G. $Li_2O–ZnO–B_2O_3$ system. *BSU Bulletin. Chemistry. Physics*. 2014;(3): 6–8. (In Russ.). Available at: https://elibrary.ru/item.asp?id=21403564

41. Khamaganova T. N., Humaeva T. G. *Method for producing lithium and zinc borate**. Patent RF No. 2550206. Publ. 2015; Bull. No 13. (In Russ.).

42. Khamaganova T. N. Synthesis of high-temperature modifications of orthoborates $LiMeBO_3$, Me = Cd, Zn*. In: *XVIII Intern. Sci. Pract. Conf. "Kulagin Readings: Technique and Technology of Processes". Pt 1*. Chita: Izdatel'stvo Zabaikal'skogo gosudarstvennogo universiteta Publ.; 2018. p. 145–149. (In Russ.).

43. Khamaganova T. N. *Method for obtaining borate α-$LiCdBO_3$**. Patent RF No. 2729805. Publ. 12.08.2020; Bull. No. 23. (In Russ.).

44. Chang K.-S. $LiZnBO_3$: crystal structure. *Journal of the Korean Chemical Society*. 2001;45(3): 251–255.

45. Chen X., Yang C., Chang X., Zang H., Xiao W. Synthesis and characterization of two alkali – metal zinc borates, α-$LiZnBO_3$ and $Li_{0.48}Na_{0.52}ZnBO_3$. *Solid State Sciences*. 2009;11: 2086–2092. https://doi.org/10.1016/j.solidstatesciences.2009.08.024

46. Chen X., Wang K., Chang X., Xiao W. Syntheses and characterization of two alkaline and transition metal orthoborates, $LiMBO_3$ (M = Zn, Cd). *Solid State Sciences*. 2016;52: 132–140. http://dx.doi.org/10.1016/j.solidstatesciences.2015.12.014

47. Tsuyumoto I., Kihara A. Synthesis, characterization and charge- discharge properties of layer-structure lithium zinc borate, $LiZnBO_3$. *Materials Sciences and Applications*. 2013;4: 246–249. https://doi.org/10.4236/msa.2013.44030

48. Wang H., Wu L., Yi H., Wang B., Wu L., Gua Y., Zhang Y. Abnormal luminescent property of Mn^{2+} in α-$LiZnBO_3$:Mn^{2+}. *Dalton Transactions*. 2015; 44: 1427–1434. https://doi.org/10.1039/c4dt02626h

49. Ragupathi V., Krishnaswamy S., Panigrahi P., Subramaniam G., Nagarajan S. Spherical $LiZnBO_3$: structural, optical and electrochemical properties. *Materials Science for Energy Technologies*. 2019;2: 267–271. https://doi.org/10.1016/j.mset.2018.12.003

50. Bajoj N. S., Omarwanr S. K. Advances in synthesis and characterization of $LiMgBO_3$: Dy^{3+}. *Optik*. 2014;125: 4077–4080. https://doi.org/10.1016/j.ijleo.2014.01.110

51. Prasad K. H., Subramanian S., Sairam T. N., Amarendra G., Srinadhu E. S., Satyanarayana N. Structural, electrical and dielectric properties of nanocrystalline $LiMgBO_3$ particles synthesized by Pechini process. *Journal of Alloys and Compounds*. 2017;718: 459–470. https://doi.org/10.1016/j.jallcom.2017.05.157

52. Yerpude M. M., Chopra V., Dhoble N. S., Kadam R. M., Krupski Aleksander R., Dhople S. Y. Luminescence study of $LiMgBO_3$:Dy for γ-ray and carbon ion beam exposure. *Journal of Luminescence*. 2019;34: 933–944. https://doi.org/10.1002/bio.3694

53. Bajaja N. S., Omanwar S. K. Studies on optical properties of $LiCaBO_3$: Tb^{3+} phosphor. *Indian Journal of Pure & Applied Physics*. 2016;54: 458–462.

54. Merzhanov A. G. *Self-propagating high-temperature synthesis. Physical chemistry. Modern problems**. Yearbook. Moscow: Khimiya Publ.; 1983. p. 6–44. (In Russ.)

55. Itin V.I., Nayborodenko Yu. S. *High temperature synthesis of intermetallic connections**. Tomsk: Tomsk University Press Publ., 1989. 214 p. (In Russ.)

56. Ketsko V. A., Beresnev E. N., Chmyrev V. I., Alikhanyan A. S., Kop'eva M. A., Kuznetsov N. T. *Oxide nanopowders and oxidation-reduction reactions in gels**. Moscow: Sputnik+ Publ.; 2011. 92 p. (In Russ.)

57. Patil K. C. Advanced ceramics: Combustion synthesis and properties. *Bulletin of Materials Science*. 1993;16(6): 533–541. https://doi.org/10.1007/BF02757654

58. Thakare D. S., Omanwar S. K., Moharil S. V., Dhopt S. M., MuthalR. M. P. L., Kondawar V. K. Combustion synthesis of borate phosphors. *Optical Materials*. 2007;29: 1731–1735. https://doi.org/10.1016/j.optmat.2006.09.016

59. Aruna S. T., Mukasyan A. S. Combustion synthesis and nanomaterials. *Current Opinion in Solid State and Materials Science*. 2008;12(3-4): 44–50. https://doi.org/10.1016/j.cossms.2008.12.002

60. Bedyal A. K., Kumar V., Prakash R., Ntwaeaborwa O. M., Swart H. C. A near-UV-converted $LiMgBO_3$:Dy^{3+} nanophosphor: Surface andspectral investigations. *Applied Surface Science*. 2015;329: 40–46. https://doi.org/10.1016/j.apsusc.2014.12.056

61. Anishia S. R., Jose M. T., Annalakshmi O., Ponnusamy V., Ramasamy V. Dosimetric properties of rare earth doped $LiCaBO_3$ thermoluminescence phosphors. *Journal of Luminescence*. 2010;130: 1834–1840. https://doi.org/10.1016/j.jlumin.2010.04.019

62. Oza A. H., Dhoble N. S., Lochab S. P., Dhoble S. J. Luminescence study of Dy or Ce activated $LiCaBO_3$ phosphor for γ-ray and C^{5+} ion beam irradiation. *Journal of Luminescence*. 2015;30(7): 967-977. https://doi.org/10.1002/bio.2846

63. Gorelik V. S., Ivicheva S. N., Kargin Yu. F., Kozulin R. K., Europium superluminescence in optically transparent photonic crystals. *Inorganic Materials*. 2014;50: 150–157. https://doi.org/10.1134/S0020168514020058

64. Wu L., Bai Y., … Xu J. Analysis of the structure and abnormal photoluminescence of a red-emitting $LiMgBO_3:Mn^{2+}$ phosphor. *Dalton Transactions*. 2018;47: 13094–13105. https://doi.org/10.1039/c8dt02450b

65. Hargunani R. P., Sonekar R. P., Omanwar S. K. Synthesis and photoluminiscence properties of Er^{3+}–Yb^{3+} co-doped $LiMgBO_3$ Phosphor. *International Journal of Current Engineering and Scientific Researgch (IJCESR)*. 2018;5(1): 218–221.

66. Kazanskaya E. V., Sandomirsky P. A., Simonov M. A., Belov N.V. Crystal structure of $LiCdBO_3$*. *Report Academy of Sciences of the USSR*. 1978;238(6): 1340–1343. (In Russ.).

67. Sokolova E. V., Boronikhin V. A., Simonov M. A. Belov N. V. Crystal structure of the triclinic modification of $LiCdBO_3^*$. *Report Academy of Sciences of the USSR*. 1979;246(5): 1126–1129. (In Russ.).

68. Bondareva O. S., Simonov M. A., Egorov-Tismenko Yu. K., Belov N. V. Crystal structures of $LiZn[BO_3]$ and $LiMn[BO_3]$. *Soviet Physics. Crystallography*. 1978;23(3): 487–491. (In Russ.).

69. Norrestam R. The crystal structure of monoclinic $LiMgBO_3$. *Zeitschrift für Kristallographie*. 1989; 187(1-2): 103–110. https://doi.org/10.1524/zkri.1989.187.1-2.103

70. Blasse G., Grabmaier B. C. A general introduction to luminescent materials. In: *Luminescent Materials*. Berlin. Heidelberg. Springer-Verlag; 1994. p. 233. https://doi.org/10.1007/978-3-642-79017-1_1

71. Du F., Nakai Y., Tsuboi T., Huang Y., Seo H. J. Luminescence properties and site occupations of Eu^{3+} ions doped in double phosphates $Ca_9R(PO_4)_7$ (R = Al, Lu). *Journal of Materials Chemistry*. 2011; 21: 4669–4678. https://doi.org/10.1039/c0jm03324c

72. Troup G. J., *Advances in Quantum Electronics*. J. R. Singer (ed.). New York—London: 1961. p. 85.

73. Kaminsky A. A. *Physics and spectroscopy of crystals**. Moscow: Nauka Publ., 1986. 272 p. (In Russ.).

74. Sen M., Shukla R., Pathak N., … Tyagi A. K. Development of $LiMgBO_3:Tb^{3+}$ as a new generation material for thermoluminescence based personnel neutron dosimetry. *Materials Advances*. 2021;2: 3405-3419. https://doi.org/10.1039/d0ma00737d

75. Das P., Pathak N., Sanyal B., Dash S., Kadam R. M. Exploring $Na_{0.1}Sr_{9.8}Eu_{0.1}(PO_4)_6F_2$ both as a potential phosphor material and host for radioactive waste immobilization. *Journal of Alloys and Compounds*. 2019;810: 151906. https://doi.org/10.1016/j.jallcom.2019.151906

76. Gupta S. K., Pathak N., Kadam R. M. An efficient gel-combustion synthesis of visible light emitting barium zirconate perovskite nanoceramics: probing the photoluminescence of Sm^{3+} and Eu^{3+} doped $BaZrO_3$. *Journal of Luminescence*. 2016;169: 106–114. https://doi.org/10.1016/j.jlumin.2015.08.032

77. Yukihara E. G., Gaza R., McKeever S. W. S., Soares C. G. Optically stimulated luminescence and thermoluminescence efficiencies forhigh-energy heavy charged particle irradiation in Al_2O_3:C. *Radiation Measurements*. 2004;38(1): 59–70. https://doi.org/10.1016/s1350-4487(03)00251-8

78. Huang D., Zhou Y., Xu W., … Yu J. Photoluminescence properties of M^{3+} (M^{3+} = Bi^{3+}, Sm^{3+}) activated $Na_5Eu(WO_4)_4$ red-emitting phosphors for white LEDs. *Journal of Alloys and Compounds*. 2013;554: 312–318. https://doi.org/10.1016/j.jallcom.2012.11.172

79. Bedyal A. K., Kumar V., Ntwaeaborwa O. M., Swart H. C. Thermoluminescence response of 120 $MeVAg^{9+}$ and γ-ray exposed $LiMgBO_3:Dy^{3+}$ nanophosphors for dosimetry. *Ceramics International*. 2016;42: 18529–18535. https://doi.org/10.1016/j.ceramint.2016.08.191

80. Chen R. Glow curves with general order kinetics. *Journal of the Electrochemical Society*. 1969;116(9): 1254-1257. https://doi.org/10.1149/1.2412291

82. Jose M. T., Anishia S. R., Annalakshmi O., Ramasamy V. Determination of thermoluminescence kinetic parameters of thulium doped lithium calcium borate. *Radiation Measurements*. 2011;46: 1026–1032. https://doi.org/10.1016/j.radmeas.2011.08.001

83. Sonekar R. P., Gawande A. B., Ingle J. T., Omanwar S. K. Photoluminescence of a Green emitting phosphor $LiCaBO_3:Tb^{3+}$. *International Journal of Knowledge Engineering*. 2012;3(1): 53-54.

84. Ovsyankin V. V., Feofilov P. P. Cooperative sensitization of luminescence in crystals activated by rare earth ions. *JETP Letters*. 1966;4(11): 471. Available at: http://jetpletters.ru/ps/1642/article_25070.pdf

85. Chen J., Zhao J. X. Upconversion nanomaterials: synthesis, mechanism, and applications in sensing. *Sensors*. 2012;12(3): 2414-2435. https://doi.org/10.3390/s120302414

86. Auzel F. Upconversion and anti-stokes processes with *f* and *d* ions in solids. *Chemical Reviews*. 2004;104(1): 139–174. https://doi.org/10.1021/cr020357g

87. Lyapin A. A.,Gushchin S. V., Kuznetsov S. V., … Ivanov V. K. Infrared-to visible upconversion luminescence in SrF_2:Er powders upon excitation of the $^4I_{13/2}$ level. *Optical Materials Express*. 2018;8(7): 1863–1869. https://doi.org/10.1364/ome.8.001863

88. Radzhabov E. A., Shendrik R. Y. Upconversion of infrared radiation in Er^{3+}-doped alkaline-earth fluorides. *Opt. Spectrosc*. 2020;128: 1752–1757. https://doi.org/10.1134/S0030400X20110211

89. Krut'ko V. A., Ryabova A. V., Komova M. G., … Loschenov V. B. Synthesis and luminescence of ultrafine Er^{3+}- and Yb^{3+}-doped $Gd_{11}SiP_3O_{26}$ and

$Gd_{14}B_6Ge_2O_{34}$ particles for cancer diagnostics. *Inorganic Materials*. 2013;49: 76–81. https://doi.org/10.1134/s0020168513010044

90. Park S., Cho S.-H. Spectral-converting behaviors of Er^{3+}–Yb^{3+}doped YOCl phosphors. *Journal of Alloys and Compounds*. 2014;584: 524-529. https://doi.org/10.1016/j.jallcom.2013.09.118

91. Milliez J., Rapaport A., Bass M., Cassanho A., Jenssen H. P. High-brightness white-light source based on up-conversion phosphors. *Journal of Display Technology*. 2006;2(3): 307–311. https://doi.org/10.1109/jdt.2006.879183

92. Hargunani S. P. Synthesis and upconversion properties of Er^{3+}–Yb^{3+} co-doped $LiBaBO_3$ phosphor. *International Advanced Research Journal in Science, Engineering and Technology*. 2016;3(11): 216–218. https://doi.org/10.17148/IARJSET.2016.31142

93. Hargunani S. P., Sonekar R. P., Omanwar S. K. Synthesis and upconversion properties of Er^{3+}–Yb^{3+} co-doped $LiSrBO_3$ phosphor. *International Journal of Luminescence and Applications*. 2017;7(2): 382-385.

94. Guo C., Yu J., Ding X., Lai M., Ren Z., Bai J. A dual-emission phosphor LiCaBO3: Ce3+, Mn2+ with energy transfer for near-UV LEDs. *Journal of the Electrochemical Society*. 2011;158(2): J42–J46. https://doi.org/10.1149/1.3526319

95. Zhang Z.-W., Lv R.-J., Zhu X.-Y., … Wang D.-J. Investigation of luminescence properties and the energy transfer mechanism of $LiSrBO_3$:Ce^{3+}, Tb^{3+} phosphors. *Journal of Materials Science: Materials in Electronics*. 2016;27: 6925–6931. https://doi.org/10.1007/s10854-016-4646-7

96. Dexter D. L. Concentration and excitation effects in multiphonon non-radiative transitions of rare-earth ions. *Journal of Chemistry and Physics*. 1954;22(6): 1063.

97. Kharabe V. R., Oza A. H., Dhoble S. J. Synthesis, PL characterization and concentration quenching effect in $Dy^{3+}$and Eu^{3+} activated $LiCaBO_3$ phosphor. *Journal of Luminescence*. 2015;30 (4): 432–438. https://doi.org/10.1002/bio.2756

98. Beck A. R., Das S., Manam J. Temperature dependent photoluminescence of Dy^{3+} doped $LiCaBO_3$ phosphor. *Journal of Materials Science: Materials in Electronics*. 2017;28(22): 17168–17176. https://doi.org/10.1007/s10854-017-7645-4

99. Pekgozl I., Erdogmus E., Cubuk S., Basak A. S. Synthesis and photoluminescence of $LiCaBO_3$: M (M: Pb^{2+} and Bi^{3+}) phosphor. *Journal of Luminescence*. 2012;132: 1394–1399. https://doi.org/10.1016/j.jlumin.2012.01.001

100. Tamboli S., Rajeswari B., Dhoble S. J. Investigation of UV-emitting Gd^{3+}-doped $LiCaBO_3$ phosphor. *Luminescence: the Journal of Biological and Chemical Luminescence*. 2015;31(2): 551–556. https://doi.org/10.1002/bio.2994

101. Jiang L. H., Zhang Y. L., Li C. Y., Hao J. Q., Su Q. Thermoluminescence studies of $LiSrBO_3$: RE^{3+} (RE = Dy, Tb, Tm and Ce). *Applied Radiation and Isotopes*. 2010;68(1): 196–200. https://doi.org/10.1016/j.apradiso.2009.10.001

102. Wang Z.-J., Li P.-L., Yang Z.-P., Guo Q.-L., Li X. A novel yellow phosphor for white light emitting diodes. *Chinese Physics B*. 2010;19(1): 017801. https://doi.org/10.1088/1674-1056/19/1/017801

103. Li Y. C., Chang Y. H., Lin Y. F., Lin Y. J., Chang Y. S. High color purity phosphors of $LaAlGe_2O_7$ doped with Tm^{3+} and Er^{3+}. *Applied Physics Letters*. 2006;89: 081110–081113. https://doi.org/10.1063/1.2337275

104. Li L., Liu Y., Li R., Leng Z., Gan S. Tunable luminescence properties of the novel Tm^{3+}- and Dy^{3+}-codoped $LiLa(MoO_4)_x(WO_4)_{2-x}$ phosphors for white light-emitting diodes. *RSC Advances*. 2015;5: 7049–7057. https://doi.org/10.1039/C4RA15643A

105. Li P., Wang Z., Yang Z., Guo Q., Li X. Emission features of $LiBaBO_3$:Sm^{3+} red phosphor for white LED. *Materials Letters*. 2009;63: 751–753. https://doi.org/10.1016/j.matlet.2008.12.041

106. Meng F., Zhang J., Yuan G., Seo H. J. Effect of temperature on the luminescence and decay behavior of divalent europium in lithium barium borate. *Physical Status Solidi. Applications and materials science*. 2015;212: 2922–2927. https://doi.org/10.1002/pssa.201532399

107. Mahajan R., Kumar S., Prakash R., Kumar V. Synthesis and luminescent properties of Sm^{3+} activated lithium zinc borate phosphor. *AIP Conference Proceedings*. 2018.;2006: 030045. https://doi.org/10.1063/1.5051301

108. Bhargavi G. N., Khare A. Luminescence studies of perovskite structured titanates: a Review. *Optika i Spektroskopiya*. 2015;118 (6): 933–948. 2015;118(6): 933–948. https://doi.org/10.7868/s003040341506015x

* *Translated by author of the article.*

Information about the author

Tatyana N. Khamaganova, Cand. Sci. (Chem.), Associate Professor, Senior Researcher Oxide Systems Laboratories, Baikal Institute of Nature Management Siberian Branch, Russian Academy of Sciences (Ulan-Ude, Russian Federation). Baikal Institute of Nature Management Siberian Branch of the Russian Academy of sciences (Ulan-Ude, Buryatia, Russian Federation).

https://orcid.org/0000-0002-8970-1481

khama@binm.ru

Received 24.11.2022; approved after reviewing 20.02.2023; accepted for publication 15.05.2023; published online 25.09.2023.

Translated by Irina Charychanskaya